UNIVERSITY OF MALTA
Faculty of Medicine and Surgery
Department of Clinical Radiology and Nuclear Medicine

# Comparison of arterial spin labelling and dynamic susceptibility contrast perfusion MR imaging in paediatric brain tumours:

# A systematic review and meta-analysis.

by

**Stephanie Vella**

**Master of Science in Clinical Radiology**

A dissertation submitted in part fulfilment of the requirements for the
Master of Science in Clinical Radiology at the
University of Malta

Supervisor: Dr. Reuben Grech

University of Malta
June 2023

L-Università ta' Malta

**FACULTY/INSTITUTE/CENTRE/SCHOOL** UNIVERSITY OF MALTA

## DECLARATIONS BY POSTGRADUATE STUDENTS

Student's Code [redacted]

Student's Name & Surname Stephanie Vella

Course Master of Science in Clinical Radiology

Title of Dissertation
Comparison of arterial spin labelling and dynamic susceptibility contrast perfusion MR imaging in paediatric brain tumours: A systematic review and meta-analysis.

**(a) Authenticity of Dissertation**

I hereby declare that I am the legitimate author of this Dissertation and that it is my original work.

No portion of this work has been submitted in support of an application for another degree or qualification of this or any other university or institution of higher education.

I hold the University of Malta harmless against any third party claims with regard to copyright violation, breach of confidentiality, defamation and any other third party right infringement.

**(b) Research Code of Practice and Ethics Review Procedures**

I declare that I have abided by the University's Research Ethics Review Procedures. Research Ethics & Data Protection form code Not Applicable.

As a Master's student, as per Regulation 77 of the General Regulations for University Postgraduate Awards 2021, I accept that should my dissertation be awarded a Grade A, it will be made publicly available on the University of Malta Institutional Repository.

[redacted]
Signature of Student

STEPHANIE VELLA
Name of Student (in Caps)

1/6/2023
Date

02.2022

## Abstract

**Background**: Brain tumours are a leading cause of mortality in children. Accurate tumour grading is essential to plan treatment and for prognostication. Perfusion imaging has been shown to correlate well with tumour grade in adults. However, there are fewer studies in paediatric patients. Moreover, there is no consensus regarding which MR perfusion technique demonstrates the highest accuracy in the latter population.

**Aim**: To compare the diagnostic test accuracy of dynamic-susceptibility contrast and arterial spin-labelling, in their ability to differentiate between low- and high-grade paediatric brain tumours at first presentation.

**Methods**: A systematic review of the literature and metanalysis of the extracted data was performed. PRISMA guidelines were followed.

**Results**: 10 studies (7 ASL and 5 DSC) comprising 477 patients were included. The area under the curve (AUC) for the summary ROC of the combined studies was 0.866. The pooled AUC for ASL was 0.88, whilst that for DSC was 0.86. Pooled sensitivity was 0.824, 95% CI [0.757 - 0.876] for ASL and 0.789, 95% CI [0.552 - 0.919] for DSC. Pooled false positive rate was 0.204, 95% CI [0.142 0.285] for ASL and 0.203, 95% CI [0.081 - 0.425] for DSC. ASL appeared to perform better than DSC however the difference between the two studies was not statistically significant.

**Conclusion**: Whilst DSC has been used more frequently than ASL in this field, the application of ASL is increasing. ASL is a contrast-free, non-invasive technique. As the diagnostic accuracy of ASL has been shown to be comparable and not inferior to DSC, its use in the diagnostic assessment of these patients should continue to be supported, however further studies with larger numbers and standardised practice are needed.

**Keywords**: paediatric; brain; tumour; grade; MRI; perfusion

## Acknowledgements

I would like to thank my supervisor Dr. Reuben Grech for his invaluable supervision and guidance during the course of my Master's degree, and for always serving as an inspiration to me.

My gratitude also extends to Prof. Joseph Lauri, for his immense help in the statistical analysis of this project. His expertise and patience are truly remarkable.

Last but not least, a heartfelt thanks to my family and friends for their unwavering support throughout this academic journey.

# Table of Contents

## List of Tables

## List of Figures

## Abbreviations and Acronyms

AIF: arterial input function

ADC: apparent diffusion coefficient

ASL: arterial spin labelling

ATT: arterial transit time

AUC: area under the curve

DSC: dynamic susceptibility contrast

IDH mutant: isocitrate dehydrogenase mutant

rCBF  relative cerebral blood flow

rCBV  relative cerebral blood volume

MRI: magnetic resonance imaging

MTT: mean transfer time

TR: repetition time

TE: echo time

FA: flip angle

FOV: field of view

NEX:  number of excitations

SNR: signal to noise ratio

PLD: post labelling delay

ROC: receiver operating characteristics

RF: radiofrequency

VC: vascular crushers

WHO: World Health Organisation

# 1. Introduction

## 1.1 Background

Brain tumours are the most common solid tumours in the paediatric population with an incidence of 6.14 per 100,000. They are also a leading cause of mortality in this age group, surpassing other cancers and recognised as the top reason for cancer mortality in those aged between 0 and 14 years at diagnosis (Barkovich AJ, 2005; Ostrom et al., 2020; Surveillance Epidemiology and End Results (SEER) Program., 2019).

Gliomas comprise the majority of central nervous system tumours in children. Embryonal tumours and pilocytic astrocytomas are the most prevalent before 9 years of age, whilst grade 2 to 3 gliomas are most predominant until 19 years of age (Lannering et al., 2009).

Overall, the majority of gliomas are low-grade tumours with generally excellent outcomes and a reported 20-year overall survival of 87% (Bandopadhayay et al., 2014). This is largely due to the relatively recent advances in the neurosurgical field and adjuvant therapy, with improved therapeutic outcomes also seen in patients with medulloblastomas, in which the 5-year survival rate now exceeds 75%. On the other hand, the mortality in high-grade gliomas, which comprise approximately 30% of these tumours, is significantly higher. Prognosis in high-grade gliomas remains poor, with 5-year survival still disappointingly low at about 20% (Fangusaro, 2012; Pollack & Jakacki, 2011). These tumours effectively pose a serious challenge in paediatric oncology. Accurate grading of tumours prior to treatment is clinically important as it allows for appropriate planning of therapeutic approach and prognostication. Whilst the current diagnostic gold standard is histopathology from biopsy or surgical resection, there are a

number of cases where surgical access is not feasible or carries high risk. Furthermore, histopathology analysis requires a few days until results are available.

Magnetic resonance imaging (MRI) plays a major role in diagnosis, surgical planning and assessment following treatment. Conventional brain MRI in isolation is often limited in this regard, and often fails to provide sufficient diagnostic test accuracy regarding underlying tumour biology (Borja et al., 2013; Peet et al., 2012). The clinical necessity for an imaging-based assessment of tumour grade in the field of neuro-oncology has led to the development and implementation of advanced MRI techniques. These include MR spectroscopy (MRS), diffusion-weighted imaging (DWI), diffusion tensor imaging (DTI), susceptibility-weighted imaging (SWI), functional imaging, chemical saturation transfer imaging and perfusion imaging. Of the modalities providing information on the physiology of tumours, perfusion MRI is a technique aimed at assessing hemodynamic parameters, providing quantitative maps of cerebral blood flow (CBF), cerebral blood volume (CBV), and mean transit time (MTT), together with vascular permeability parameters, i.e., contrast transfer coefficient (K*trans*) (Lacerda & Law, 2009).

MR perfusion has, in the past decade, become increasingly relevant in brain tumour assessment, given the established use of anti-angiogenic and anti-vascular therapies, (Farid et al., 2014) as well as for its ability to provide information regarding long-term survival (Hipp et al., 2011) and tumour grade, as shall be discussed in detail in Chapter 2.

There are currently three main MR perfusion modalities, namely dynamic susceptibility contrast (DSC) and dynamic contrast enhanced (DCE) perfusion imaging, both of which require the use of an exogenous contrast agent, and arterial spin labelling (ASL) which

utilises an endogenous tracer. Of these, DSC and ASL are routinely used. DCE is less well-studied, particularly in the paediatric population, and shall therefore not be considered in this review.

Whilst these imaging techniques have been well studied in adult patients, there is less targeted research specifically relating to paediatric patients and no clear consensus of the clinical role of these techniques. This is especially relevant when considering the fact that the biological features of paediatric brain tumours are unique. The recently published 2021 update of the WHO Classification of Tumours of the Central Nervous System, includes a number of notable changes (WHO Classification of Tumours Editorial Board., 2021). In particular, for the first time, the 2021 WHO classification divides diffuse gliomas into adult-type and paediatric-type neoplasms. More than ever before, the differences between paediatric and adult brain tumours are being recognised, compelling the undertaking of targeted research in this regard.

The purpose of this study is to compare the diagnostic test accuracy of the two most widely used MRI perfusion techniques; dynamic susceptibility contrast and arterial spin labelling, in their ability to differentiate between low- and high-grade paediatric brain tumours at first presentation. A concise review of the literature regarding the classification of paediatric brain tumours, as well as the technical aspects and recent developments of these two MR perfusion methods is presented. The up-to-date relevant literature on the application of MR perfusion in paediatric tumour grading will be systematically reviewed and data regarding accuracy will be extracted from selected appropriate studies. This data will then be synthesised and analysed to ascertain if these techniques can accurately determine different tumour grades, and if one technique is superior to the other.

# 2. Literature review

## 2.1 Classification of CNS tumours

Tumours of the CNS have been traditionally classified according to location, patient age at presentation and histological type. However recent advances in molecular biology and genetics have allowed for a more comprehensive subgrouping. The 2021 WHO classification of Tumours of the Central Nervous System represents the sixth version of the international standard and continues to advocate the role of molecular diagnostics, whilst retaining other established tumour characterisation methods, including histology and immunohistochemistry.

Primary tumours of the CNS are divided into the following main categories: gliomas, glioneuronal and neuronal tumours; embryonal tumours; choroid plexus tumours; pineal tumours; cranial and paraspinal nerve tumours; meningioma; mesenchymal, nonmeningothelial tumours; melanocytic tumours; haematolymphoid tumours; germ cell tumours and sellar region tumours (Louis et al., 2021). Some of the key points in relation to paediatric neuroimaging will be subsequently highlighted.

**Gliomas, glioneuronal and neuronal tumours**

As previously stated, the new classification recognises that there are tangible clinical and molecular differences between gliomas that primarily occur in adults and those occurring in children.

There are thus three subtypes of diffuse gliomas;

- adult-type diffuse gliomas, which comprise astrocytoma IDH-mutant, oligodendroglioma IDH-mutant and 1p/19q-codeleted, and glioblastoma, IDH-wildtype.
- paediatric-type diffuse low-grade gliomas.
- paediatric-type diffuse high-grade gliomas.

Paediatric-type diffuse low-grade gliomas include diffuse astrocytomas, MYB or MYBL1-altered; diffuse low-grade gliomas, MAPK pathway–altered; angiocentric gliomas and polymorphous low-grade neuroepithelial tumour of the young (PLNTY).

MAPK pathway–altered diffuse low-grade gliomas include most tectal plate gliomas, being IDH- and H3-wildtype. These lesions almost always demonstrate up-regulation of the RAS/MAPK pathway, with a spectrum of FGFR1 and BRAF mutations. They also lack histologic features of malignancy and molecular alterations such as CDKN2A/B mutations (Ryall et al., 2020).

Angiocentric gliomas are rare tumours, typically presenting with intractable focal epilepsy. They appear as cortically based T2-hyperintense masses, typically located in the temporal or frontal lobes. Reported distinguishing imaging features include the presence of intralesional high T1 signal areas, a stalk-like appearance and atrophy of the regional brain parenchyma (Kurokawa et al., 2022).

PLNTY is a recently recognised entity characterised by oligodendroglioma-like histology, variable morphology and alterations in the MAPK-pathway. Radiologically it typically manifests as a well-delineated supratentorial T2-hyperintense lesion, the most

common location being the temporal lobe. The presence of central calcification and peripheral cystic components is characteristic (Y. Chen et al., 2020).

Paediatric-type diffuse high-grade gliomas are further classified into the following four subtypes based on molecular features:

- diffuse midline glioma, H3 K27-altered
- diffuse hemispheric glioma, H3 G34-mutant
- diffuse paediatric-type high-grade glioma, H3-wildtype
- IDH-wildtype and infant-type hemispheric glioma

Of note, the classic diffuse intrinsic pontine gliomas, manifesting as expansile T2-hyperintense lesions are most commonly H3K27-altered diffuse midline gliomas. Additionally, unilateral or bilateral thalamic lesional involvement is commonly seen with these gliomas, together with aggressive local spread and early metastatic dissemination (Aboian et al., 2017).

Infant-type hemispheric gliomas are typically seen in the first year of life. They usually occur in a supratentorial location, and are large, sometimes even holo-hemispheric heterogenous lesions, often demonstrating intra-tumoural haemorrhage. These gliomas exhibit molecular mutations involving the receptor tyrosine kinases ALK, ROS1, NTRK, MET (Guerreiro Stucklin et al., 2019).

Circumscribed astrocytic gliomas are characterised as such by their comparatively more solid growth pattern and include the well-known pilocytic astrocytoma, pleomorphic xanthoastrocytoma, subependymal giant cell tumours and chordoid gliomas. Two new

entities have been introduced in the recent classification; high-grade astrocytomas with piloid features and MN1-altered astroblastoma.

High-grade astrocytomas with piloid features have been noted to arise in the posterior fossa in adult patients with neurofibromatosis type 1. These tumours differ from the typical paediatric pilocytic astrocytomas. They exhibit CDKN2A/B deletions, possess a distinct DNA methylation profile and have a much poorer prognosis (Bender et al., 2021).

Astroblastomas are typically superficial, supratentorial, relatively well-circumscribed lesions with a multicystic or "bubbly" appearance and little, if any, surrounding vasogenic oedema. The presence of MN1 alterations (a transcriptional coregulator involved in the development of meningiomas and acute myeloid leukaemia) is used to define the lesion (W. Chen et al., 2020).

Since the implementation of molecular characterisation, there has been a significant advancement in the treatment of low-grade gliomas. Most notably identification of BRAF V600E mutations allows targeted therapy using BRAF inhibitors. Dabrafenib plus trametinib has recently been approved by the FDA for the treatment of BRAF V600E low-grade gliomas (Wen et al., 2022) .

Glioneuronal/neuronal tumours are a varied group of tumours characterised by neuronal differentiation and include the following: ganglioglioma, desmoplastic infantile ganglioglioma/astrocytoma (DIG), dysembryoplastic neuroepithelial tumour (DNET), diffuse leptomeningeal glioneuronal tumour, dysplastic cerebellar gangliocytoma and neurocytomas. The following three entities have been added in the updated classification: myxoid glioneuronal tumour, diffuse glioneuronal tumour with oligodendroglioma-like

features and nuclear clusters (DGONC) and multinodular and vacuolating neuronal tumour (MVNT).

Ependymal tumours, which represent 5–10% of all childhood primary brain tumours are the third most frequently occurring paediatric brain cancer. More than 90% of ependymomas originate in the brain (mostly commonly infratentorially), with the remainder arising in the spinal cord. They are classified into four histological groups: subependymoma, myxopapillary, classic and anaplastic. The latter two are the most frequently seen in children (Udaka & Packer, 2018). Ependymomas are now further classified depending on location, as well as histological and molecular features, which have been shown to correlate with outcome.

On imaging, posterior fossa ependymomas demonstrate a lobulated heterogenous appearance, often containing cystic changes and/or calcifications. They typically arise from the body or inferior fourth ventricle with classical extension through the foramen of Magendie and the foramina of Luschka. Infratentorial ependymomas are now classified as group PFA or group PFB based on their DNA methylation profile. Group A tumours are hypermethylated and are mostly found in infants and young children. They are associated with a poorer outcome when compared to Group B tumours. With regards to spinal cord ependymomas, apart from the classic myxopapillary variant, a new entity defined by the presence of MYCN amplification is now recognised. It is seen more commonly in adults and associated with early dissemination and a poor prognosis (Louis et al., 2021).

Supratentorial ependymomas fall into another two major subgroups: ZFTA fusion-positive and YAP1 fusion-positive. The former occurs in children and adults and is seen

as relatively well demarcated mixed solid-cystic lesion on imaging. YAP1 fusion-positive ependymomas usually occur in children below the age of 3 years and have a better prognosis (Ellison et al., 2020).

**Embryonal tumours**

CNS embryonal tumours are divided into two groups: medulloblastoma and other CNS embryonal tumours.

Medulloblastomas are the most common malignant brain tumours in children and comprise up to 20% of all paediatric brain tumours (Ostrom et al., 2020). In the past, classification was based on histology with the following four recognised categories: classic, desmoplastic/nodular, medulloblastoma with extensive nodularity (MBEN), and large cell/anaplastic. The current classification incorporates both histology and molecular profiling based on DNA methylation or transcriptome profiling. The following four distinct subgroups have been established: WNT-activated, SHH-activated and TP53 wild-type, SHH-activated and TP53-mutant, and non-WNT/non-SHH (Louis et al., 2021).
The WNT-activated subtype occurs mostly in older children and accounts for about 10% of medulloblastomas. Based on imaging studies, the cerebellar peduncle and cerebellopontine angle appear to be the most characteristic locations, however these tumours can be located anywhere in the posterior fossa. They are thought to arise from the lower rhombic lip, are usually of classic histology and have the most favourable prognosis of all four groups. Metastases are rare at presentation, and the 5-year survival rate is 95% (Reis et al., 2021).

The SHH-activated/TP53 wild-type medulloblastoma is the second commonest subtype comprising approximately 30% of medulloblastomas overall. It mainly occurs in infants

and adults, being rare in children. These tumours appear to arise from granule neuron progenitor cells in the upper rhombic lip and are thus typically located in a cerebellar hemisphere, however may also occur in the midline. This subgroup is the most heterogenous in terms of its biologic, pathological and clinical characteristics. SHH-1 and SHH-2 subgroups most frequently demonstrate desmoplastic or MBEN histology, whilst SHH-3 and SHH-4 subgroups usually exhibit classic or large-cell anaplastic histology.

SHH-activated/TP53-mutant medulloblastoma is the rarest subtype and confers the worst overall prognosis. It typically occurs in children with a predilection for males and is highly aggressive in nature with a propensity to metastasize.

The non-WNT/non-SHH subtype represents 50%–60% of all medulloblastomas, making it the most common of the four groups. This entity incorporates the former group 3 and group 4 medulloblastomas and is further divided into eight subgroups based on methylation profiling. These medulloblastomas can be found in all locations, classically in the midline around the fourth ventricle, and often exhibit minimal or no enhancement (Osborn et al., 2022).

Other embryonal tumours

This group includes embryonal tumour with multi-layered rosettes (ETMR), atypical teratoid/rhabdoid tumour (ATRT), as well as a few new tumour types: CNS tumour with BCOR internal tandem duplication, FOXR2-activated CNS neuroblastoma, and the provisional entity cribriform neuroepithelial tumour (Louis et al., 2021).

ETMRs occur in infants and children below the age of four years. They are seen on imaging studies as large, heterogeneous masses with relatively well-defined margins and

high cellularity and restricted diffusivity of the solid components. The vast majority are supratentorial in location. Necrosis and intra-tumoural haemorrhage are commonly seen and the enhancement pattern is highly variable.

ATRT usually present as a posterior fossa mass, however also frequently arise supratentorially. The vast majority of cases occur in young children less than two years of age. It is also typically a large heterogenous mass, and it may be difficult to distinguish it from ETMR on imaging (Shih & Koeller, 2018).

CNS neuroblastoma peaks at about 5 years of age, being characterised genetically by FOXR2 gene alterations, and histologically by neuronal differentiation, increased vascularity, presence of necrosis and endothelial proliferation. The imaging appearance is that of a large, heterogeneous supratentorial mass with prominent cysts, necrosis, little surrounding oedema, and variable enhancement. CNS tumours with BCOR internal tandem duplication, are malignant tumours seen in children and adolescents, typically in the cerebral or cerebellar hemispheres. As yet only a small number of cases describing imaging findings have been reported in the literature (Osborn et al., 2022).

## 2.2 Dynamic Susceptibility Contrast

Dynamic susceptibility contrast imaging is the most commonly used MR perfusion technique. It involves the injection of a gadolinium-based contrast agent through a large gauge cannula followed by rapid tracking of the bolus via MR imaging (Calamante, 2013). Many centres administer a preload, i.e., a third of the total contrast dose prior to the dynamic study. This serves to reduce effects of contrast leakage T1 effects, which is particularly relevant in the imaging of brain tumours as will be discussed later. After a delay of about 5 minutes, the remainder of the contrast is injected at a rate of 3-5 mL/s

(Jahng et al., 2014). The passage of contrast causes a susceptibility gradient between the intravascular and extravascular compartments by means of local distortions in the main magnetic field, resulting in a transient loss of signal intensity in the vicinity of vessels.

The rapidly varying signal changes that are generated are measured using ultrafast imaging sequences. The most frequently used method is the T2*-weighted gradient-echo (GRE) echo planar imaging (EPI), which is sensitive to vessels of all diameters. Alternatively, T2-weighted images, obtained with spin-echo (SE) EPI methods can also be applied, with the advantage of minimising artifact at interfaces between brain and bone or air and of being more sensitive to signal changes at a microvascular level, such as capillaries, rather than that in larger vessels, such as cortical veins. The latter technique however requires larger contrast doses (Simonsen et al., 2000).

The signal-time course data for each voxel is converted into tracer tissue concentration-time course data. This conversion uses the assumption that the concentration of gadolinium is proportional to the noted change in T2*-relaxation rate ($\Delta R2^* = 1/\Delta T2^*$), which in turn is proportional to the negative logarithm of relative signal intensity:

$$[Gd] \propto \Delta R2^* = -\frac{1}{TE} 1n\left(\frac{S_t}{S_0}\right)$$

In the above formula, $S_0$ represents the baseline signal intensity in a given voxel, whilst $S_t$ is the signal at time *t* during passage of the contrast agent bolus (Rosen et al., 1989).

Measurement of the flow of the cerebral blood is based on the concept that the capillary bed is a linear system. Following the instantaneous injection of contrast agent into the arterial system at time 0, some of the contrast particles will travel through a direct pathway to the venous side of the capillary bed, whilst other particles will take longer and

more tortuous routes. This results in a dispersion of the contrast agent particles within the tissue and a range of particle transit times. The percentage of injected contrast remaining in the tissue at time *t* after an instantaneous injection is known as the residue, the function of which can be expressed as a curve, starting at 1 and washing out over time until no contrast remains in the tissue. Tissues with rapid transition of contrast will have sharp and narrow residue curves, whilst those with prolonged transition time will have a wide residue curve. The area under the curve represents the average transition time of a contrast agent particle through the capillary bed, known as the mean transit time (MTT).

In practice however, instantaneous delivery of contrast agent to the brain is not possible, unless direct carotid injection is performed. A number of factors including cardiac output, vessel calibre and confirmation as well as injection rate and dispersion, influence and delay the delivery of contrast agent to the studied tissue. In order to address this, measurement of the arterial input function (AIF) is performed allowing correction for the injection profile and dispersion of the contrast agent. The AIF may be obtained directly from the imaging data by manually selecting the voxels in or near a large artery, such as the middle cerebral artery. This method is referred to as global AIF and is applied to all voxels within a slice. However, an appreciable distance may exist between the site of AIF measurement and the voxel of interest. This may result in errors in haemodynamic quantification due to bolus delay and dispersion of contrast. A potentially superior approach is to identify several local AIF arising from small arteries located very close to each of the tissue voxels being imaged. The main reservation of this approach is the fact that partial volume artefact may arise due to the small vessel size (Calamante et al., 2004).

Through the mathematical process of convolution, the individual instantaneous contrast agent residues at various time delays after injection are scaled using individual AIF and

integrated together to generate the tissue contrast concentration curve. Thus, when performing DSC perfusion, the AIF and contrast concentration curve can be directly measured. The tracer concentration-time curves are then deconvolved with the AIF for each voxel in the brain, resulting in an estimate of the residue function. This is then analysed to determine various tissue hemodynamic parameters. The initial height of the deconvolved tissue concentration-time curve equates to the cerebral blood flow (CBF) and integrating the area under curve allows determination of the cerebral blood volume (CBV). The mean transit time (MTT) may then be calculated as the ratio of CBV to CBF. Additionally, the time point where the maximum concentration of the bolus is reached is referred to as the time to peak (TTP) (Østergaard et al., 1996). Many deconvolution algorithms have been developed, with the most commonly used being singular value decomposition, Fourier transformation and statistical inference methods (Fieselmann et al., 2011).

Of note these parameters are dependent on a number of factors, related to the bolus injection, as well as variables within the patient being imaged, such as total-body vascular volume and cardiac output. Thus, the obtained haemodynamic measurements cannot be directly compared between different patients, and may even vary between different examinations of the same patient. Intra and intrasubject comparison is made possible by using an internal reference standard, such as normal appearing grey or white matter, allowing semiquantitative or relative values to be obtained (Petrella & Provenzale, 2000).

The data analysis methods described assume that the contrast agent which is injected remains within the intravascular compartment and that for this reason the T1 effects may be ignored. However, in several brain tumours this is not the case, as they cause a

breakdown of the blood-brain barrier and leakage of contrast into the extracellular extravascular space (EES), thus altering the resulting signal in two competing ways. The T1 value of the EES is shortened, resulting in an increase in signal which competes with the intravascular signal, leading to an underestimation of CBV. Conversely, the change in susceptibility differences between the intravascular compartment and the EES causes a decrease in signal and failure to return to baseline and hence an overestimation of CBV. A potential approach to mitigating adverse T1 effects resulting from contrast leakage is to administer a single-dose preload of contrast before the acquisition of the DSC data, during which a second dose of contrast is administered. This serves to reduce the concentration gradient between the intravascular and extravascular compartments that drives the extravasation of contrast, thus lowering the T1 of the extravascular compartment (Leu et al., 2017). In one study it was shown that a single-dose preload (0.1 mmol Gd/kg) with a 5-minute incubation time before the examination dose, resulted in the best distinction in rCBV between tumor and treatment effect (Hu et al., 2010).

Careful selection of sequence parameters and post-processing techniques is also useful to minimise the effect of contrast leakage on the signal-time course. In fact, in another study even though contrast agent preload was used, valid correlation with tumour grade was only achieved when post-processing leakage correction was applied (Schmainda et al., 2004). The Boxerman technique is the most widely used post-processing method that allows correction of CBV by using the signal-time course obtained from a whole brain mask of non-enhancing pixels in order to correct the leakage affected DSC signal-time course. A parameter representing the amount of leakage that has taken place, referred to as K2, is also acquired (Boxerman et al., 2006).

## 2.3 Arterial Spin Labelling

Arterial spin labelling is an MR perfusion technique that employs the use of radiofrequency (RF) pulses to non-invasively label protons within arterial blood allowing it to act as endogenous tracer. Following labelling of spins within a labelling plane and a specified time interval, an image of the brain within the acquisition plane is obtained; termed the tagged image. Subsequently the same image of the brain without the application of a RF pulse is obtained; termed the control image. Kinetic model estimations are then used to calculate quantitative cerebral blood flow (CBF) maps, using the perfusion-weighted image rendered from the signal difference between the tagged and control images (Williams et al., 1992).

Usually, the relative difference between the control and labelled images is quite low, resulting in a low signal-to-noise ratio (SNR) and thus poor quality of the final CBF images. This is ameliorated by acquiring many repetitions of the control and label images (Haller et al., 2016).

There are two main techniques used for labelling: pulsed and continuous (Alsop et al., 2015). In pulsed ASL (PASL), there is instantaneous inversion of all the proton spins within a wide slab upon the application of discontinuous RF pulses. PASL techniques can be further classified into those where spin labelling is done asymmetrically with respect to the plane of imaging (EPISTAR, PICORE) or symmetrically (FAIR). Conversely, in continuous ASL (CASL) there is a continuous application of an RF field within a thin labelling plane, resulting in the flow-driven inversion of proton spins as they pass through the labelling plane. A more recently developed variation of CASL is pseudo-continuous ASL (pCASL), whereby a short train of RF pulses is used instead of a continuous one, mimicking its effect. This technique offers high labelling efficiency and provides a higher

SNR and reproducibility than that achieved using pulsed ASL (Dai et al., 2008). Furthermore, pCASL allows for a reduced absorption rate and thus a lower tissue energy deposition and magnetization transfer when compared to CASL (Kitajima & Uetani, 2023).

With regards to image acquisition, particular parameters to be considered are the read-out technique, use of background suppression and the time interval between labelling and image acquisition. Fast read-out methods, usually with multi-slice 2D EPI or alternatively segmented 3D methods (3D GRASE or stack-of-spirals) are used. Whilst the latter provide higher SNR and spatial resolution, they are more sensitive to motion when compared to 2D methods.

Background suppression is achieved through the application of additional RF pulses between the labelling phase and image readout, minimising the static spins and thus reducing the background tissue signal with minimal effect on the perfusion component. In this way, the unfavourable effect of head motion on a CBF image is reduced (Garcia et al., 2005).

Vascular crushing (VC) is a further suppression technique that results in the elimination of intra-arterial signals i.e., macrovascular spins, through the application of magnetic field gradients which result in the dephasing of fast-flowing blood. This increases the sensitivity of ASL to the microvasculature resulting in a more accurate measurement of true capillary blood flow. However, the routine use of VC is not recommended in clinical practice, as besides decreasing SNR, it may mask evidence of pathological delayed or collateral flow, as well as arteriovenous shunting (Ferré et al., 2013; Ye et al., 1997).

A critical parameter in ASL concerns the time interval between spin labelling and image readout, referred to as post-labelling delay (PLD). When single delay acquisitions are used, enough time should be allowed for the labelled protons to reach the tissues in the imaging slice by the time read-out occurs. However, caution is required, as if this time is too long the majority of measurable tracers may decay.

Another important factor to take into consideration is the mean arterial transit time (ATT), which refers to the time taken for labelled blood to flow from the labelling region to the tissue being studied. This value varies depending on the patient, and the PLD should ideally be set just after the longest ATT in any given patient. When the PLD is shorter than ATT, the labelled blood that has not reached the tissue can be seen as ATT/macrovascular artifacts (i.e. labelled blood seen at the level of the proximal arteries, instead of in the microvasculature or tissue) and so-called signal void (i.e. the labelled blood which does not reach the distal voxels in time leaves an area devoid of signal). This phenomenon limits accurate assessment of CBF, however may be a sign of an underlying stenosis proximally or collateral pathways as a cause for the delay in arrival of the labelled blood (Jezzard et al., 2018).

Multi-delay ASL has been developed as a means to ameliorate this issue and allow more accurate quantification of CBF and ATT (Wang et al., 2013). This technique provides information about the temporal dynamics of the arrival of labelled spins to tissue by using a kinetic model following sampling of multiple delays. A considerable disadvantage of this form of acquisition is that it is rather time-consuming as each time step has to be acquired separately. Each MRI vendor has developed a slightly different approach to multi-delay ASL with varying durations and SNR. The first to be developed was the

Look-Locker encoding for PASL (Günther et al., 2001), followed by the multi-TI technique and Hadamard encoding (Golay & Ho, 2022).

ASL processing involves multiple phases. Briefly, the first stage consists of data conversion and sharing and prepares the data for the actual image processing. The second stage involves processing of structural data, including lesion correction, segmentation and normalisation. This is followed by ASL data processing which itself requires several preparatory steps, including motion correction, exclusion of outlier corrupted control-label pairs, registration of ASL to structural images, and $M_0$ processing. These steps are followed by CBF quantification and optional partial volume correction (Clement et al., 2022).

As stated above, the actual perfusion-weighted image is generated from the subtraction of the label images from the control images. This subtraction image is then quantified i.e., converted to physiological values to obtain a CBF image in milliliters of blood per 100 grams of tissue per minute (mL/100g/min). This quantification requires the use of a perfusion calibration image ($M_0$ image) which serves as a baseline reference to provide information on the basic tissue magnetisation. The following equations are used, depending on whether PASL (a) or pCASL (b) is being undertaken:

(a) $$CBF = 6000 \frac{\lambda}{2\alpha} \frac{\Delta M}{M_0} \frac{e^{\frac{TI}{T_{1b}}}}{TI_1} [\text{mL/min/100g}]$$

(b) $$CBF = 6000 \frac{\lambda}{2\alpha} \frac{\Delta M}{M_0} \frac{e^{\frac{PLD}{T_{1b}}}}{T_{1b}\left(1-e^{-\frac{\tau}{T_{1b}}}\right)} [\text{mL/min/100g}]$$

The factor 6000 is used to set the units of mL per min per 100g of tissue. The term $\lambda/2\alpha$ scales the blood flow, whereby $\lambda$ is the correction factor that accounts for the difference

between the $T_1$ of blood and the $T_1$ of brain tissue and α is the tagging efficiency. ΔM refers to the difference between the labelled and control images normalised by the proton density-weighted image $M_0$. In both equations, $T_{1b}$ is the blood $T_1$ relaxation time. For the PASL calculation, TI is the time between labelling and acquisition whilst $TI_1$ is the interval between labelling and the application of a saturation pulse. In pCASL, τ refers to the labelling duration time, whilst PLD is the subsequent time interval prior to acquisition which allows the labelled spins to clear the intravascular space (Golay & Ho, 2022).

Several of these factors, particularly the labelling duration and the blood $T_1$, may influence CBF quantification. Therefore, these must be suitably taken into account during image processing, as any incorrect definition of these parameter values may strongly affect the resulting CBF data (Clement et al., 2022).

A white paper published on the topic (Alsop et al., 2015) provides guidance regarding the optimal protocols for clinical practice in both paediatric and adult patients. It clearly recommends the use of pCASL with a segmented 3D readout and a higher magnetic field strength, i.e., 3T for optimal SNR. Labelling parameter references are also provided, adjusted for patient age. Of note PLD should be set to 2000ms in neonates and 1500ms in children in order to account for differences in blood velocity, with blood flow being faster in the latter age group.

## 2.4 Role of Perfusion Imaging

Neuroimaging plays an indispensable role in the diagnosis, treatment, and monitoring of paediatric brain tumors. Whilst the conventional contrast-enhanced MRI is good at detecting brain tumours, it has its limitations in the assessment of tumour grade and histological correlation, as it relies largely on the presence of blood-brain barrier

breakdown. However, besides the fact that a lesion that enhances may not be a tumour, not every tumour that enhances is high-grade and not every high-grade tumour enhances (Borja et al., 2013; Peet et al., 2012). As reported in one study, 89% of low-grade tumours may demonstrate enhancement, whilst up to 8% of medulloblastomas do not (Porto et al., 2014). Diffusion imaging with ADC analysis, which has now practically become part of conventional imaging, may provide additional valuable information about tumour cellularity and architecture, however studies have shown that it is again not completely reliable in predicting tumour grade or histology (Poretti et al., 2012).

Angiogenesis is an important pathogenic mechanism in tumour growth and does not correspond with the degree of enhancement (Averill & Kandula, 2017). This is where perfusion techniques play a major role, being well-suited to evaluate neovascularization of brain tumours.

Traditionally, DSC and ASL have been thought to have complementary roles in perfusion imaging of brain tumours, with ASL on the one hand being more sensitive to absolute quantification of tumour blood flow, and DSC on the other hand being more sensitive to alterations in tissue permeability and capillary blood volume. Nevertheless, a comparison of their respective ability to assess tumour grade remains a valid research topic due to a number of clinically relevant differences between these techniques.

DSC perfusion imaging has proven to be useful in the pre-treatment evaluation of adult intracranial neoplasms, by indicating tumour grade, guiding biopsy, and estimating prognosis (Law et al., 2003, 2007; Morita et al., 2010; Shin et al., 2002). In addition, a number of studies have shown that ASL could be an alternative to DSC in the assessment

of brain tumours in adults (Ata et al., 2016; Cebeci et al., 2014; Hirai et al., 2011; Järnum et al., 2010; Luan et al., 2020; Warmuth et al., 2003; Wolf et al., 2005).

Since the conception of perfusion imaging, DSC has been used more frequently than ASL for tumour evaluation in the paediatric population (Cha, 2006; Dallery et al., 2017; Ho et al., 2015; Koob et al., 2016; Lucas et al., 2018; Withey et al., 2022). However, the application of ASL in children has significantly increased in the past few years for a number of reasons. ASL is a completely non-invasive technique and does not require the administration of gadolinium-based contrast agents. This makes it ideal for scenarios where contrast is contraindicated or best avoided, such as in renal impairment, history of anaphylactic reactions against contrast and paediatric patients in general. This is especially relevant in light of the evidence that administration of contrast results in accumulation of gadolinium in the brain, even in patients without severe renal impairment (Kanda et al., 2015; McDonald et al., 2015). It is also useful where venous access is difficult or not feasible, as is oftentimes the case in young children, particularly those on chemotherapy. It additionally aids in scenarios where repeated examinations are necessary, such as in cases of failed sedation or patient motion.

On the other hand, DSC relies on reasonably high contrast doses, particularly when correcting for leakage effects, and requires the use of a high-flow power injector and large calibre venous access, posing considerable technical challenges in young patients. Bolus delay and dispersion caused by slow injection rates may lead to underestimation of CBF values. Furthermore, in the case of an inadequate study as is quite frequent in young children, it is not possible to repeat DSC in the same examination without a further bolus administration of contrast agent. ASL on the other hand does not require leakage calculation and correction (Kitajima & Uetani, 2023).

As a technique, DSC is extremely vulnerable to image distortion and susceptibility artifacts from interfaces of brain with bone or air, and those resulting from the presence of blood products and calcium (Romano et al., 2012). In ASL susceptibility effects causing signal dropout and geometric distortions are comparatively less prominent as shorter echo times are used. It may therefore be better suited in the evaluation of paediatric brain tumours adjacent to the skull base. As paediatric patients possess a higher cerebral water content and overall, more cerebral blood flow than adults, a higher SNR and reduction in artifacts can be afforded in ASL studies in this population (Kerner et al., 2022).

Mirroring the adult trend, a number of paediatric studies have emerged in recent years, showing ASL to be comparable to DSC in the grading of paediatric brain tumours (Dangouloff-Ros et al., 2016; Hales et al., 2013, 2019; Kikuchi et al., 2017; Liu et al., 2015; Morana et al., 2017, 2018; Piccardo et al., 2019; Testud et al., 2021; Vidyasagar et al., 2016; Yeom et al., 2014).

# 3. Research Methodology

## 3.1 Criteria for considering studies for inclusion

The Patients, Interventions, Comparisons and Outcomes (PICO) model was used to define the research question for this study (Richardson et al., 1995). The scope was to assess if there is a significant difference in the diagnostic test accuracy of dynamic-susceptibility contrast and arterial spin-labelling, in their ability to differentiate between low- and high-grade paediatric brain tumours at first presentation. A summary of the inclusion and exclusion criteria is provided in Table 1.

Types of studies

Cross-sectional studies with retrospective or prospective design published from 2012 onwards were included. Case-control studies, case reports, qualitative studies, grey literature and literature reviews were excluded. Non-English literature studies were eligible for inclusion.

Participants

Studies that comprised a cohort of paediatric patients (younger than 18 years) with brain tumours were considered. As this review aimed to assess grading of brain tumours at first presentation, studies enrolling patients who had undergone previous surgical intervention or received any oncological treatment prior to the index test were excluded. The main target condition was gliomas, however studies which included other non-glial brain neoplasms were also considered. In this review, high grade tumours were considered disease positive, and low-grade tumours disease negative. Animal studies were excluded.

Index tests

Studies in which pre-operative MR imaging comprising DSC and/or ASL perfusion were included. All ASL and DSC techniques were considered eligible for inclusion. Studies utilising only DCE MR perfusion were excluded, as this method has not been routinely used in clinical practice in this field.

Gold standard test

In order to be eligible for inclusion, studies required subsequent histologic tumour diagnosis and WHO grade classification following biopsy or resection. Exception to this criterion was made in cases of optic pathway glioma and diffuse midline glioma, in which biopsy is not routinely performed for diagnosis due to their eloquent location.

| | Inclusion criteria | Exclusion criteria |
|---|---|---|
| Study design | • Peer reviewed studies based on original data analysis.<br>• Published from 2012 onwards. | • Grey literature.<br>• Literature reviews, case reports or case controls. |
| Participants | • Human subjects below the age of 18.<br>• Diagnosis of brain tumour.<br>• Treatment naïve. | • Adult only or mixed adult and paediatric subjects.<br>• Previously treated with radiotherapy and/or chemotherapy |
| Index test | • ASL and/or DSC MRI perfusion.<br>• Availability of result data. | • DCE perfusion.<br>• No author response to inquiry for data clarification. |
| Gold standard test | • Histologic assessment following biopsy or resection (except in cases of optic pathway/brainstem glioma).<br>• Use of WHO classification for tumour grading. | • No histological diagnosis. |

***Table 1 - Inclusion and exclusion criteria***

## 3.2 Search Strategy including PRISMA flowchart

This metanalysis was undertaken in accordance with the Cochrane Handbook for Diagnostic Test Accuracy Reviews (Leeflang et al., 2013). The Preferred Reporting Items for Systematic Reviews and Meta-Analyses (PRISMA) 2009 guidelines (Moher et al., 2009) were also followed.

A systematic search strategy for quantitative data literature was developed. The following search string was used: ("Glioma" OR "neoplasm" OR "neoplasia" OR "tumor" OR "tumour" OR "cancer" OR "malignancy" AND "Brain" OR "Central Nervous System" OR "Cerebral" OR "intracranial" OR "Glial") AND ("paediatric" OR "pediatric" OR "young adult" OR "infant" OR "child" OR "children" OR "adolescent") AND ("perfusion" OR "ASL" OR "arterial spin labelling" OR "arterial spin labeling" OR "arterial spin labeled" OR "dynamic susceptibility contrast" OR "DSC" OR "Perfusion Weighted MRI" OR "MR Perfusion" OR "MRI Perfusion" OR "Spin Labels").

Articles were retrieved from the following three electronic databases: MEDLINE (Ovid) [Appendix 1], Web of Science Core Collection [Appendix 2] and SCOPUS [Appendix 3]. The search only considered human studies and was limited to studies in the last 10 years. The most recent search for this review was run on 5 August 2022.

Retrieved hits were transferred onto an online systematic review screening tool (Ouzzani et al., 2016). Following the removal of duplicates, the remaining articles were assessed for inclusion independently by two researchers with 10 years' and 1 years' experience in meta-analyses, respectively. In addition, the references from chosen articles were manually reviewed with the aim of identifying any further potentially relevant studies which were not detected in the initial search.

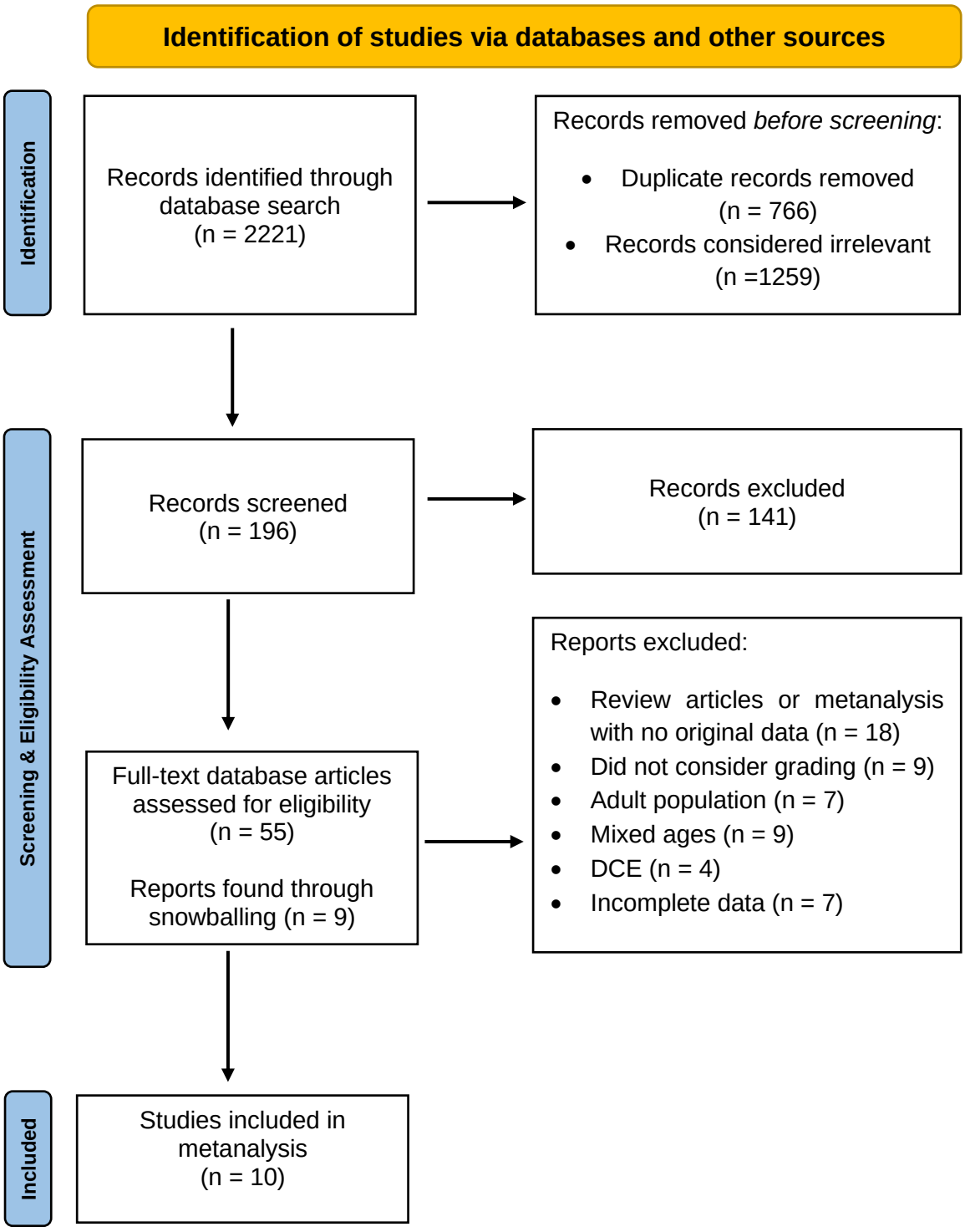


***Figure 1** - Preferred Reporting Items for Systematic Reviews and Meta-Analyses (PRISMA) flow chart of the study inclusion process*

### 3.3. Selection of studies

The systematic database search yielded a total of 2221 records. Following the removal of 766 duplicates, two review authors independently performed preliminary screening of titles and excluded 1259 irrelevant records. The remaining 196 records were screened for inclusion in the meta-analysis. After title and abstract assessment 141 articles were excluded, with 55 articles remaining for full-text evaluation. In addition, another 9 articles were obtained through references and assessed for inclusion.

Following full-text evaluation, 51 studies were excluded for the following reasons: Eighteen records were review articles or metanalyses lacking original quantitative data. Nine studies did not consider tumour grading but rather disease progression, overall survival or aimed to assess the technical aspects of the perfusion techniques. In seven of the reports the study population was adult, whilst nine of the studies included both adult and paediatric patients with no possibility of separating the respective results. Finally, in seven of the remaining studies, quantitative data values were not reported. The respective authors were contacted and requested to provide this information; however, no response was received. Ten studies that included a total of 477 patients were included in the meta-analysis. The flowchart of retrieval process is presented in Figure 1.

### 3.4 Data extraction

The following data was extracted independently by two researchers from each of the included studies onto a pre-set sheet.

General information: Study title, first author, journal, country of origin, year of publication and study design (prospective vs. retrospective).

Patient information: Sample size, age range, type of brain tumours being studied and tumour WHO grade.

Imaging information: MR scanner model, manufacturer and field strength, method of MR perfusion performed, ASL technique (pseudo-continuous or pulsed), DSC bolus regime, imaging parameters including TR, TE, slice thickness, matrix size, field of view, flip angle, labelling duration and post-labelling delay (the latter in the case of ASL), region of interest (ROI) evaluation technique and reference region used.

Quantitative results: Data regarding rCBV, rCBF, sensitivity, specificity, receiver operating characteristic (ROC) curve with the corresponding area under the curve (AUC) value, extracted based on authors' pre-specified and recommended thresholds.

### 3.5 Overview of Critical Appraisal Tools used

Each of the included studies was critically appraised based on the revised Quality Assessment of Diagnostic Accuracy Studies tool (QUADAS 2) (Whiting, 2011). Two review authors independently extracted information from each study based on the published articles and any available supplementary material.

The following four domains were assessed: patient sampling, index test, reference standard and flow and timing. Each domain was evaluated in terms of risk of bias, and the first three with regards to concerns in applicability. Signaling questions (*yes/no/unclear*) were included to assist in judgments, using an adapted template [Table 2] created by the authors of a previously published metanalysis to fit the assessment of included studies (Delgado et al., 2018). Any incongruities were dealt with through discussion with a third senior clinician.

| **Risk of Bias** |
|---|
| |
| Patient selection: |
| • Low if consecutive or reported in years of inclusion together with clear inclusion criteria. |
| • Unclear if no mention of consecutive series of patients or inclusion/exclusion criteria. |
| • High if a non-consecutive series was reported and inappropriate inclusion/exclusion criteria were used. |
| |
| Index test: |
| • Low if perfusion MRI was interpreted blinded. |
| • Unclear if no information on blinding but a predefined cut-off was specified for a positive test. |
| • High if an exploratory cut-off was used and no information on blinding was given. |
| |
| Reference standard: |
| • Low if reported on a blinded evaluation and WHO adherence. |
| • Unclear if no information on blinding was given. |
| • High if reported on an unblinded evaluation. |
| |
| Flow and timing: |
| • Low if less than 30 days between perfusion MRI and histopathology. |
| • Unclear if not reported. |
| • High if reported after 6 months. |
| |
| **Applicability Concerns** |
| |
| Patient selection: |
| • Low if mixed tumour types. |
| • Unclear if tumour types were not reported or only 1 tumour type was reported. |
| • High if other comparisons than between high- and low-grade were given. |
| |
| Index test: |
| • Low if presented as relative CBF/CBV and pseudo-continuous used if ASL. |
| • Unclear if CBF/CBV was not normalised. |
| • High if perfusion metrics other than CBF were presented or if pulsed ASL was used. |
| |
| Reference standard: |
| • Low if tumours were classified according to WHO 2007 or later. |
| • Unclear if WHO was used but the year was unspecified. |
| • High if no report on the histopathologic diagnosis classification system |
| |

***Table 2 - Adapted critical appraisal assessment***

## 3.6 Data Analysis

The pooled rCBF and rCBV values for low- and high-grade tumours obtained by ASL and DSC respectively were used to generate box plots and statistical significance testing was performed.

All analyses were performed using R Statistical Software (v4.2.2 Patched (2022-11-10 r83330) (R Core Team., 2021). The sensitivities and specificities obtained from each study were used to calculate the true-positive, true-negative, false-positive, and false-negative count. A case was defined as a histologically proven high-grade tumour. A positive index test implied a diagnosis of a high-grade tumour, while a negative test suggested a low-grade tumour. Thus, true positives were correctly diagnosed high-grade tumours, false negatives were high-grade tumours incorrectly labelled as low-grade tumours, true negatives were correctly diagnosed low-grade tumours, while false positives were low-grade tumours incorrectly labelled as high-grade tumours.

Between-study heterogeneity variance was measured by tau-squared ($\tau^2$) and I-squared ($I^2$) values. The random-effect model was used to merge statistics. Significance level was set at $p < 0.05$. Forest plots showing pairs of sensitivity and specificity, with their 95% confidence intervals, were constructed for each study using Metafor (Viechtbauer, 2010).

The bivariate model (Reitsma et al., 2005) was applied in order to account for between-study variability in estimates of sensitivity and specificity through the inclusion of random effects for the logit sensitivity and logit specificity parameters of the bivariate model. The reitsma function of the mada package was used to generate the bivariate model parameters required to construct the summary ROC (SROC) plot from the obtained data-sets (Doebler, 2022). The AUC for the SROC of all studies was estimated to

determine the overall diagnostic test accuracy of perfusion MRI, followed by a separate comparison of the SROC of ASL versus DSC studies. Crosshairs were constructed from confidence intervals for each point in the ROC space.

# 4. Results

## 4.1 Introduction

Collectively, the ten studies included in this metanalysis reported 477 patients with brain tumours/gliomas. All studies were retrospective and avoided case-control design. The sample size per study was generally adequate and ranged from 19 to 117 cases. Only one study had a sample size of less than 20 (Kikuchi et al., 2017). The studies were conducted in the following countries: France (n = 3), Italy (n = 3), United Kingdom (n = 2), United States of America (n = 1) and Japan (n = 1).

The following tumour types were assessed across all studies: gliomas and glioneuronal tumours (n=304), ependymomas (n=41), embryonal (n=115), haemangioblastoma (n=1), germ cell (n=1), craniopharyngioma (n=4), choroid plexus (n=7), pineal (n=3), chordoma (n=1). All cases but one diffuse midline glioma received histological diagnosis. Hence, the bulk of the tumours were of the glial and embryonal groups, which reflects their incidence. The vast majority of the included studies used the 2016 WHO brain tumour classification.

DSC was used in three of the included studies, whilst ASL was the perfusion technique assessed in five studies. Two of the included studies used both DSC and ASL. In 4 of the ASL studies, the pulsed technique was used, with the remaining being pseudo-continuous. None of the DSC studies used contrast agent pre-loading. Information regarding arterial input function was only available in two out the five DSC studies, where it was automated. The majority of examinations were performed on a 1.5T scanner (in four studies), one study used a 3T scanner and five studies used both.

## 4.2 Characteristics of Included Studies

The basic information of the included literature is presented in Table 3. Details pertaining to each study follow.

| First author, Publication year | Region | No. of cases | Median /Mean age | Glioma Grade *n* | Field strength | Perfusion Technique | Diagnostic Parameters |
|---|---|---|---|---|---|---|---|
| Dallery 2017 | France | 30 | 9.4 | 11 LG, 19 HG | 1.5 & 3T GE | DSC | rCBF, rCBV |
| Dangouloff-Ros 2016 | France | 117 | 6.2 | 52 LG, 65 HG | 1.5T GE | ASL | rCBF |
| Hales 2019 | UK | 32 | 4.5 | 13 LG, 19 HG | 1.5 & 3T Siemens | ASL | rCBF |
| Ho 2014 | USA | 63 | 6.3 | 38 LG, 25 HG | 1.5 & 3T Siemens | DSC | rCBV |
| Kikuchi 2017 | Japan | 19 | 6 | 11 LG, 8 HG | 3T Philips | ASL | rCBF |
| Morana 2017 | Italy | 26 | 9.5 | 12 LG, 14 HG | 1.5T Philips | ASL | rCBF |
| Morana 2018 | Italy | 37 | 9 | 22 LG, 15 HG | 1.5T Philips | ASL & DSC | rCBF, rCBV |
| Piccardo 2019 | Italy | 22 | 9 | 10 LG, 12 HG | 1.5T Philips | ASL | rCBF |
| Testud 2021 | France | 46 | 7 | 15 LG, 31 HG | 1.5 & 3T Siemens | ASL & DSC | rCBF, rCBV |
| Withey 2021 | UK | 85 | 8 | 45 LG, 40 HG | 1.5 & 3T Various | DSC | rCBV |

***Table 3 - Overview of study characteristics***

### 4.2.1 Dallery 2017

**Study design and setting,**

Retrospective. January 2010 - December 2016. France.

**Patient sampling characteristics**

Total no. of patients: 30

Average age: 9.4 years. 13 female, 17 male

Tumour types: 22 glioma/glioneuronal, 8 embryonal

**Index tests**

Perfusion technique: DSC

Perfusion parameters: rCBV

Scanners: 1.5T (Optima MR450W, GE Healthcare, Milwaukee, WI) and 3T (Signa MRHDx, GE Healthcare, Milwaukee, WI)

Acquisition parameters: single shot gradient-echo EPI. At 3T: TR: 1500ms; TE: 30ms; FA, 60°. At 1.5T: TR 1500-2500 ms, TE, 30-65 ms; FA: 60°-90 °. NSA, FOV, Partitions & Matrix: NA

Use of contrast preload: No

Post-processing algorithm: Gamma-variate function

ROI method: Manual ROI in maximal lesion CBV. Normalised to contralateral normal white matter.

**Target condition and reference standard**

All cases had histological diagnosis. WHO classification 2016. 11 LG, 19 HG.

### 4.2.2 Dangouloff-Ros, 2016

**Study design and setting**

Retrospective. March 2011- March 2015. France.

**Patient sampling characteristics**

Total no. of patients: 117

Median age: 6.2 years (2.6–11.1). 48 female, 81 male

Tumour types: 71 glioma/glioneuronal or neuronal, 12 ependymal, 45 embryonal, 1 haemangioblastoma

**Index tests**

Perfusion technique: pseudo-continuous ASL

Perfusion parameters: rCBF

Scanners: 1.5T (Signa HD, GE Healthcare, Milwaukee, WI)

Acquisition parameters: TR: 4428ms, TE:10.5ms, PLD: 1025ms; Partitions: 80, FOV: 240mm, Matrix: 512x512; FA: 155°, Acquisition time: 257s

Post-processing algorithm: NA

ROI method: Centred on highest tumour rCBF value. Normalised to normal grey-matter in cerebellum (posterior fossa tumours)/temporal lobe (supratentorial tumours).

**Target condition and reference standard**

All cases had histological diagnosis. WHO classification 2007. 52 LG, 65 HG.

### 4.2.3 Hales, 2019

**Study design and setting**

Retrospective. June 2015- Sept 2017. United Kingdom.

**Patient sampling characteristics**

Total no. of patients: 32

Median age: 4.8 years (0.4 - 14.5 years). 17 female, 15 male

Tumour types: 24 gliomas/glioneuronal, 7 embryonal, 1 germ cell

**Index tests**

Perfusion technique: pseudo-continuous ASL

Perfusion parameters: relative/normalised CBF

Scanners: 1.5T (Magnetom Avanto, Siemens, Erlangen, Germany) & 3T (Magnetom Prisma, Siemens, Erlangen, Germany)

Acquisition parameters: 3D gradient-and-spin-echo readout, labelling duration:1800ms, PLD: 1500ms.

Post-processing: Matlab (MathWorks Inc., Natick, MA)

ROI method: Manual ROI in maximal lesion CBF. Normalised to contralateral normal grey matter

**Target condition and reference standard**

All cases (with the exception of one diffuse midline glioma) had histological diagnosis. WHO classification 2016. 13 LG, 19 HG.

### 4.2.4 Ho, 2014

**Study design and setting**

Retrospective. September 2009 - August 2013. USA.

**Patient sampling characteristics**

Total no. of patients: 63

Mean age: 6.3 years (1.0–16.8). 24 female, 39 male

Tumour types: 36 gliomas/glioneuronal or neuronal, 10 ependymal, 13 embryonal, 1 craniopharyngioma, 1 pineal, 2 choroid plexus papilloma

**Index tests**

Perfusion technique: DSC

Perfusion parameters: rCBV

Scanners: 1.5T & 3T (Avanto and Verio, Siemens, Erlangen, Germany)

Acquisition parameters: Gradient-echo EPI. TR 1410–2250ms, TE 30–45ms, FA: 90°

NSA, FOV, Partitions & Matrix: NA

Use of contrast preload: No

Post-processing algorithm: NA

ROI method: Manual ROI in maximal lesion CBV. Normalised to contralateral normal white matter.

**Target condition and reference standard**

All cases had histological diagnosis. WHO classification 2007. 38 LG, 25 HG.

### 4.2.5 Kikuchi, 2017

**Study design and setting**

Retrospective. January 2013 - September 2014. Japan.

**Patient sampling characteristics**

Total no. of patients: 19

Median age: 6 years (2 months –12 years). 9 female, 10 male

Tumour types: 9 glial/glioneuronal, 4 ependymal, 3 embryonal, 2 craniopharyngioma, 1 choroid plexus papilloma

**Index tests**

Perfusion technique: pseudo-continuous ASL

Perfusion parameters: rCBF

Scanners: 3T (Achieva TX, Philips Healthcare, Best, the Netherlands)

Acquisition parameters: 2-dimensional gradient-echo echo-planar imaging. TR: 4200ms, TE: 8.6ms, NEX: 32, PLD: 1525ms, FOV: 240mm, Matrix: 64x64; Acquisition time: 277s. FA & Partitions: NA.

Post-processing algorithm: NA

ROI method: Manual ROI in maximal lesion CBF. Normalised to contralateral grey matter.

**Target condition and reference standard**

All cases had histological diagnosis. WHO classification 2016. 11 LG, 8 HG.

### 4.2.6 Morana, 2017

**Study design and setting**

Retrospective. Timeframe not specified. Italy.

**Patient sampling characteristics**

Total no. of patients: 26

Median age: 9.5 years (2–17). 11 female, 15 male

Tumour types: gliomas

**Index tests**

Perfusion technique: pulsed ASL

Perfusion parameters: rCBF max

Scanners: 1.5T (Intera Achieva; Philips, Best, the Netherlands)

Acquisition parameters: multi-slice single-shot echo planar imaging (EPI) readout with parallel imaging (SENSE factor = 2.3) TR: 4000ms; TE: 25ms; FA, 40°, FOV: 240mm, Matrix: 80x77, 30 label/control pairs; labelling slab thickness: 100mm, 20mm gap, PLD: 1450 - 1800ms, Acquisition time: 245s, Partitions: NA

Post-processing algorithm: NA

ROI method: Manual ROI in maximal lesion CBF. Normalised to contralateral normal white matter.

**Target condition and reference standard**

All cases had histological diagnosis. WHO classification 2016. 12 LG, 14 HG.

### 4.2.7 Morana, 2018

**Study design and setting**

Retrospective. 2010-2016. Italy.

**Patient sampling characteristics**

Total no. of patients: 37

Median age: 9 years (2–17). 19 female, 18 male

Tumour types: gliomas

**Index tests**

Perfusion technique: DSC and pulsed ASL

Perfusion parameters: rCBV and rCBF

Scanners: 1.5T (Intera Achieva; Philips, Best, the Netherlands)

Acquisition parameters: *DSC*: T2*-weighted single-shot gradient-recalled echo-planar imaging (GRE EPI). TR: 1912ms, TE: 40ms; FA: 75°, Matrix: 128×128, FOV: 240mm, NEX: 1, Acquisition time: 84s. *ASL*: Signal targeting and alternating radiofrequency (EPISTAR) and multislice single-shot echo planar imaging (EPI) readout with parallel imaging (SENSE factor = 2.3). TR: 4000ms, TE: 25ms, FA: 40°, Matrix: 80×77, FOV: 240mm; 30 label/control pairs; labelling slab thickness: 100mm, 20mm gap, PLD: 1500-1800ms, Acquisition time: 248s. No VC.
Use of contrast preload: No

Arterial input function: Determined automatically using cluster analysis techniques.

Post-processing algorithm: Olea Sphere, version SP 3.0, Olea Medica

ROI method: Manual ROI in maximal lesion CBF. Normalised to contralateral normal grey matter.

**Target condition and reference standard**

All cases had histological diagnosis. WHO classification 2016. 22 LG, 15 HG.

### 4.2.8 Piccardo, 2019

**Study design and setting**

Retrospective. 2010-2018. Italy.

**Patient sampling characteristics**

Total no. of patients: 22

Median age: 9 years (4 - 17). 10 female, 12 male

Tumour types: gliomas

**Index tests**

Perfusion technique: pulsed ASL

Perfusion parameters: rCBF max

Scanners: 1.5T (Intera Achieva; Philips, Best, the Netherlands)

Acquisition parameters: Signal targeting and alternating radiofrequency (EPISTAR) and multislice single-shot echo planar imaging (EPI) readout with parallel imaging (SENSE factor = 2.3). TR: 4000ms, TE: 25ms, FA: 40°, Matrix: 80×77, FOV: 240mm; 30 label/control pairs; labelling slab thickness: 100mm, 20mm gap, PLD: 1500-1800ms, Acquisition time: 248s. No VC.

Post-processing algorithm: NA

ROI method: Manual ROI in maximal lesion CBF. Normalised to contralateral normal grey and white matter.

**Target condition and reference standard**

All cases had histological diagnosis. WHO classification 2016. 10 LG, 12 HG.

### 4.2.9 Testud, 2021

**Study design and setting**

Retrospective. May 2015 - January 2020. France.

**Patient sampling characteristics**

Total no. of patients: 46

Mean age: 7 years. 24 female, 22 male

Tumour types: 28 glioma/glioneuronal, 6 ependymal, 12 embryonal

**Index tests**

Perfusion technique: DSC and pulsed ASL

Perfusion parameters: rCBV, rCBF

Scanners: 1.5 (Aera, Siemens, Erlangen, Germany) & 3T system (Skyra, Siemens, Erlangen, Germany)

Acquisition parameters: DSC: At 3T: TR: 2350ms; TE: 23ms; FA: 90°. At 1.5T: TR 1610ms, TE; 30ms; FA:90°. ASL: At 3T: labelling duration: 700ms, PLD: 1400 - 1900ms, TR: 5000ms, TE: 18.28ms, FA: 180°. At 1.5T: labelling duration: 700ms, PLD: 1800ms, TR: 4000ms, TE: 36.32ms, FA: 180°. No VC. NSA, FOV, Partitions & Matrix: NA

Use of contrast preload: No

Arterial input function: Determined automatically using cluster analysis techniques.

Post-processing algorithm: Olea Sphere software (v. SP3.0 16, Olea Medical, Canon)

ROI method: Manual ROI in maximal lesion CBV. Normalised to contralateral normal white matter.

**Target condition and reference standard**

All cases had histological diagnosis. WHO classification 2016. 15 LG, 31 HG

### 4.2.10 Withey, 2021

**Study design and setting**

Retrospective. Multicentre – 4 centres. November 2005 - May 2017. UK.

**Patient sampling characteristics**

Total no. of patients: 85

Mean age: 8 years. 37 female, 48 male

Tumour types: 41 glioma/glioneuronal or neuronal, 27 embryonal, 9 ependymal, 4 choroid plexus tumour, 1 craniopharyngioma, 1 chordoma, 2 pineoblastoma

**Index tests**

Perfusion technique: DSC

Perfusion parameters: rCBV

Scanners and acquisition parameters: Various as demonstrated below.

| Center | 1 | | 2 | 3 | 4 | | |
|---|---|---|---|---|---|---|---|
| Scanner type | Siemens Avanto | Philips Achieva | Siemens Verio | Philips Achieva | Philips Achieva | Philips Achieva | Philips Achieva |
| Field strength | 1.5 T | 3 T | 3 T | 3 T | 1.5 T | 3 T | 3 T |
| Head coil | 12-element head | 32-channel | 32-channel | SENSE head-8 | SENSE-NV-16 | SENSE head-8 | SENSE head-8 |
| Sequence | GE-EPI | GE-EPI | GE-EPI | GE-EPI | sPRESTO | sPRESTO | GE-EPI |
| TR (ms) | 1,490–1,643 | 1,830–1,865 | 1,570 | 1,666–2,343 | 16.7–17.2 | 15.5–16.0 | 582–1,866 |
| TE (ms) | 40 | 40 | 29 | 40 | 24.7–25.2 | 23.5–24.0 | 18.4–40.0 |
| Flip angle (°) | 20 | 20 | 45 | 75 | 7 | 7 | 20–40 |
| Slice thickness (mm) | 5.0 | 3.5 | 3.5 | 4.0 | 3.5 | 3.5 | 3.5–7.0 |
| No. slices | 19–21 | 30 | 16 | 25–35 | 30–36 | 30–34 | 30 |
| No. dynamics | 60 | 60 | 60 | 40 | 60 | 60 | 40–60 |
| Field-of-view (mm) | 230×230 | 240×240 | 220×220 | 224×224 | 220×220 | 230×230 | 240×240 |
| Matrix | 96×96 | 96×96 | 64×64 | 128×128 | 64–80×64–80 | 128×128 | 96×96 |
| SENSE? | Y | Y | N | Y | Y | Y | Y |
| Temporal resolution (s) | 1.5–1.6 | 1.8–1.9 | 1.6 | 1.7–2.3 | 1.3–1.6 | 1.2–1.4 | 0.6–1.9 |
| Total scan time (s) | 90–99 | 110–112 | 94 | 67–94 | 77–94 | 71–83 | 70–118 |
| Pre-bolus | Y | Y | N | Y | Y ($n$=12), N ($n$=15), NA ($n$=9) | | |

ROI method: Manual ROI in maximal lesion CBV. Normalised to contralateral normal white matter.

**Target condition and reference standard**

All cases had histological diagnosis. WHO classification 2002, 2007, 2016. 45 LG, 40 HG

## 4.3 Appraisal of Included Studies

The methodological quality assessment of each of the included studies (according to the modified QUADAS-2 criteria) is summarised in Table 4.

| Study, Publication year | Risk of Bias | | | | Applicability Concerns | | |
|---|---|---|---|---|---|---|---|
| | Patient Selection | Index Test | Reference Standard | Flow and Timing | Patient Selection | Index Test | Reference Standard |
| Dallery 2017 | + | - | ? | ? | + | + | + |
| Dangouloff-Ros 2016 | + | + | + | ? | + | + | + |
| Hales 2019 | + | + | ? | ? | + | + | + |
| Ho 2014 | + | - | ? | ? | + | + | + |
| Kikuchi 2017 | + | - | ? | ? | + | + | + |
| Morana 2017 | + | - | ? | ? | + | - | + |
| Morana 2018 | + | - | ? | ? | + | - | + |
| Piccardo 2019 | + | - | ? | ? | ? | - | + |
| Testud 2021 | + | + | ? | ? | + | - | + |
| Withey 2021 | + | - | ? | ? | + | + | + |

***Table 4 - Methodological quality assessment***

***+ indicates low risk ? indicates unclear risk - indicates high risk***

None of the included studies had low risk of bias and low concern for applicability across all domains, however all were deemed to be of eligible quality.

Participant Selection: Risk of bias was low in nine out of ten studies. The remaining study was deemed as unclear risk due to lack of information on patient sampling (Kikuchi et

al., 2017) . Concerns of applicability with regard to participant selection were low in nine out of ten studies. In one study only one tumour type was studied (Piccardo et al., 2019).

Index test: The highest level of risk of bias was observed in this test domain, with seven studies not specifying blinding procedures for interpretation of perfusion data and applying the exploratory cut-off determination. High risk of applicability concern was found in four studies, attributable to the use of pulsed ASL (Morana et al., 2017, 2018; Piccardo et al., 2019; Testud et al., 2021).

Reference standard: Only one study was deemed to have low risk of bias by specifying the use of blinding in histopathological assessment (Dangouloff-Ros et al., 2016). The remaining studies did not describe blinding of interpretation and were deemed as unclear risk. Applicability concerns were low across the included studies, with all patients undergoing a resection or biopsy. The WHO classification from 2007 onwards was used as the reference standard in all cases.

Flow and timing: This domain was deemed as unclear risk of bias throughout, as none of the studies provided information regarding the interval period between the index test and reference standard.

## 4.4 Findings of Included Studies

The average rCBV/rCBF values per tumour grade in each included study are presented in Table 5. All tumours were graded using the WHO classification, and in this review high-grade tumour cases were classified as disease positive, and low-grade tumours as disease negative for the quantitative analysis.

| Study | No. of cases | Glioma Grade *n* | Perfusion Technique | Diagnostic Parameters | Low grade | High grade |
|---|---|---|---|---|---|---|
| Dallery 2017 | 30 | 11 LG, 19 HG | DSC | rCBF<br>rCBV | 0.87 ± 0.41<br>0.99 ± 0.50 | 2.37 ± 1.38<br>2.69 ± 1.35 |
| Dangouloff-Ros 2016 | 117 | 52 LG, 65 HG | ASL | rCBF | 0.68 ± 0.24 | 1.74 ± 1.45 |
| Hales 2019 | 32 | 13 LG, 19 HG | ASL | rCBF | n/a | n/a |
| Ho 2014 | 63 | 38 LG, 25 HG | DSC | rCBV | 0.99 ± 0.53 | 1.48 ± 0.95 |
| Kikuchi 2017 | 19 | 11 LG, 8 HG | ASL | rCBF | 0.69 ± 0.81 | 1.76 ± 0.95 |
| Morana 2017 | 26 | 12 LG, 14 HG | ASL | rCBF | 0.81 ± 0.56 | 2.08 ± 0.98 |
| Morana 2018 | 37 | 22 LG, 15 HG | ASL & DSC | rCBF<br>rCBV | 0.59 ± 0.27<br>0.49 ± 0.33 | 1.37 ± 0.26<br>1.51 ± 0.34 |
| Piccardo 2019 | 22 | 10 LG, 12 HG | ASL | rCBF | 1.20 ± 0.49 | 1.89 ± 0.45 |
| Testud 2021 | 46 | 15 LG, 31 HG | ASL & DSC | rCBF, rCBV | n/a | n/a |
| Withey 2021 | 85 | 45 LG, 40 HG | DSC | rCBV | 1.68 ± 1.36 | 2.54 ± 1.63 |

***Table 5 - Relative/normalised CBV & CBF values per tumour grade***

### 4.4.1 Box Plots

The cut-off rCBF and rCBV values obtained from each of the included studies (where these were available) were pooled and are illustrated as box-plots below [Figure 2]. The pooled rCBF and rCBV of high-grade tumours were higher than those of low-grade tumours, with the results being statistically significant.

Paired t-test for DSC values: t value for (high-grade scores) – (low-grade scores) is t = 4.0197, df = 3, p-value = 0.0277. This difference is thus significant at the 0.05 level, with a 95% CI of [0.2119, 1.8230]. The sample estimates for this mean difference between high-grade and low-grade scores is: 1.018.

Paired t-test for ASL values: t value for (high-grade scores) – (low-grade scores) t = 9.234, df = 4, p-value = 0.0008. Therefore, this difference is significant at the 0.001 level with a 95% CI of [0.6811, 1.2669]. The sample estimates for this mean difference between high-grade and low-grade scores is: 0.974.

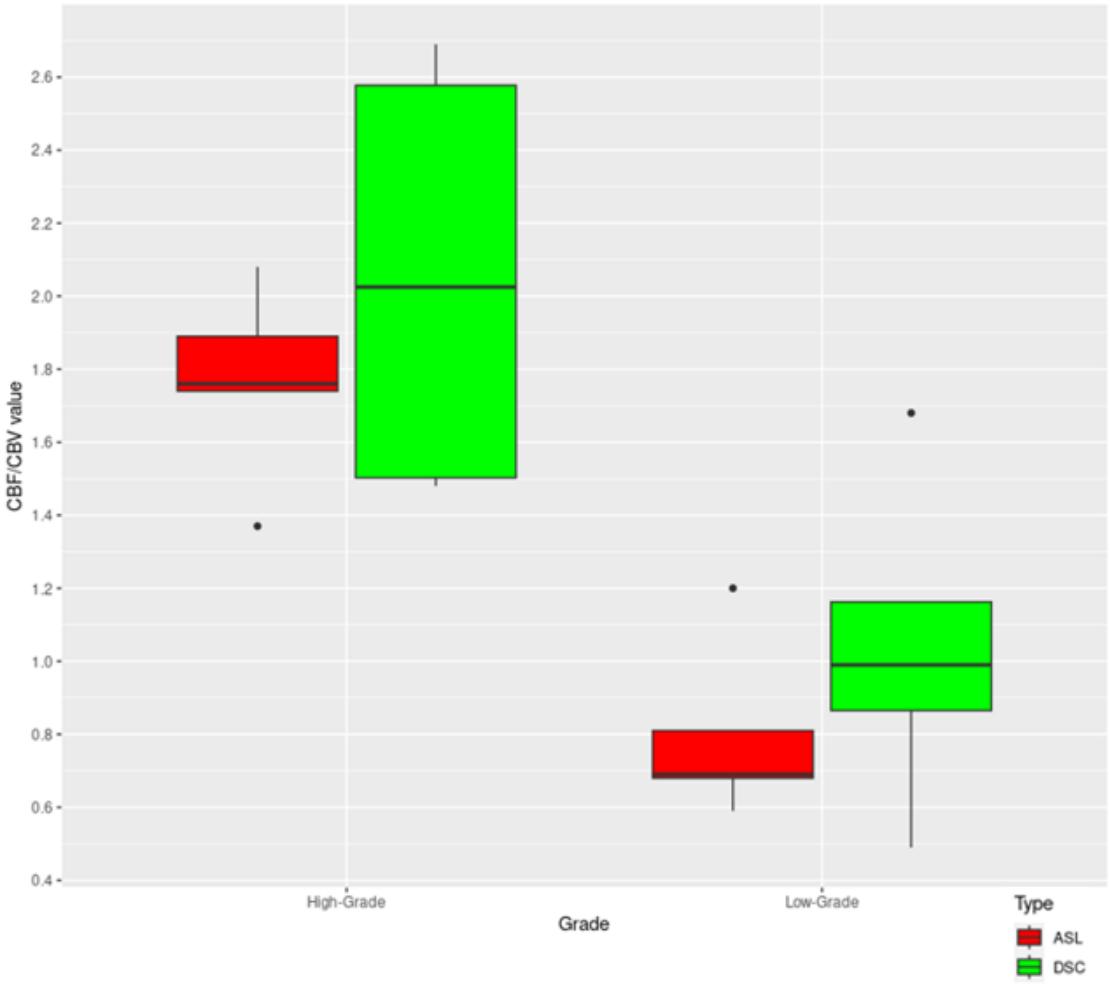


***Figure 2 - rCBF values for ASL and rCBV values for DSC from included studies***

### 4.4.2 Forest Plots for Sensitivity and Specificity

With regards to sensitivity of ASL [Figure 3], the between-study heterogeneity variance as measured by $\tau^2$ was negligible, indicating strong homogeneity between the studies. The pooled sensitivity was 0.867 with a 95% confidence interval (CI) equal to [0.806 - 0.911]. In terms of specificity of ASL [Figure 4], although the between-study heterogeneity variance was higher, as estimated by $\tau^2$= 0.536 and $I^2$ = 0.536, these figures were not statistically significant (p value=0.36). The pooled value of the specificity was 0.825 with a 95% CI = [0.687 - 0.910].

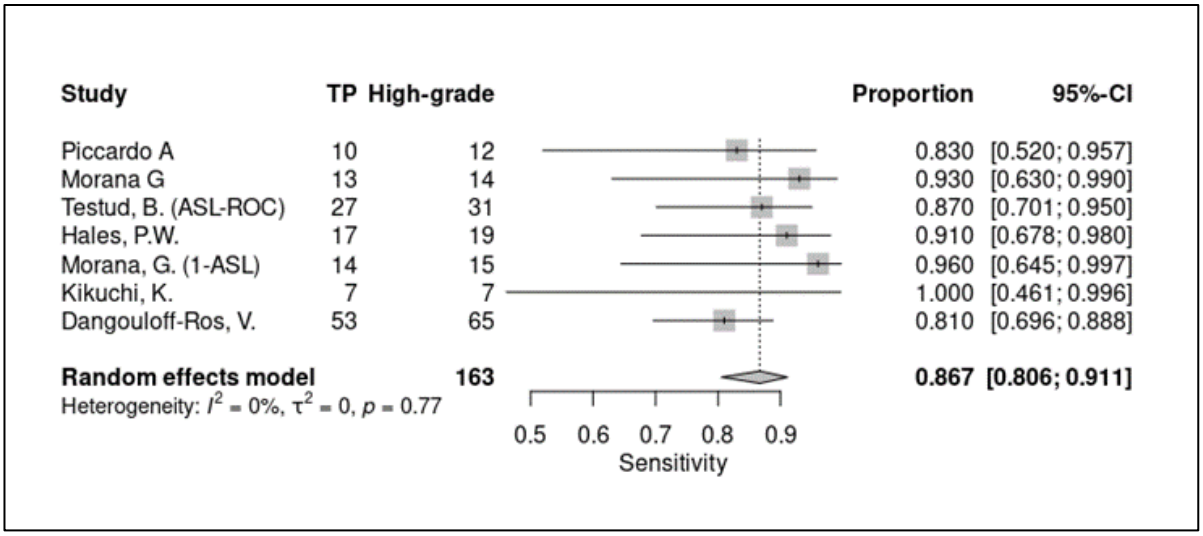


***Figure 3 - Sensitivity plot for ASL***

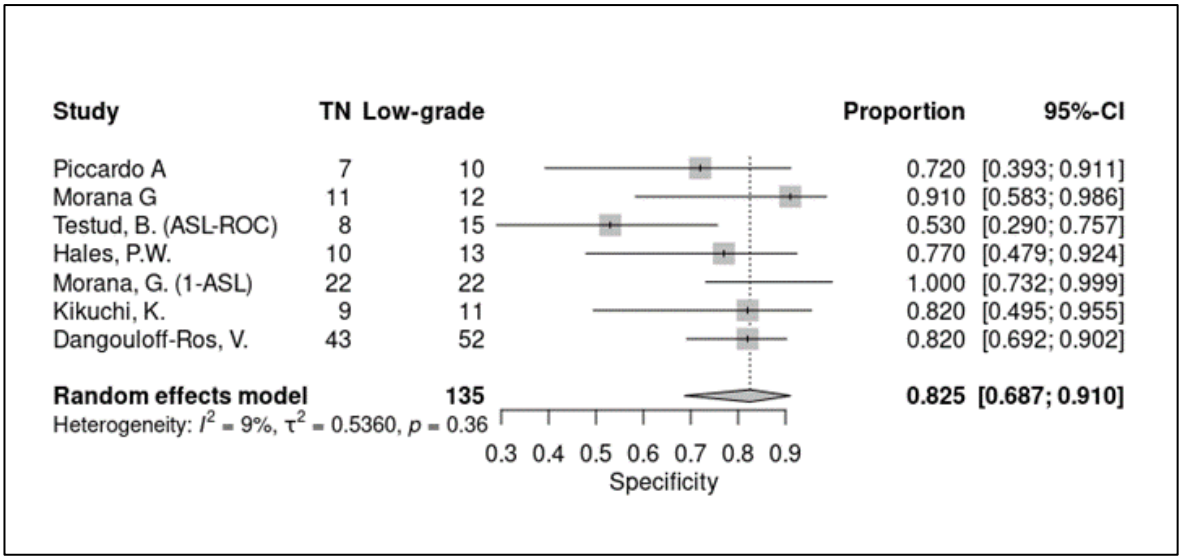


***Figure 4 - Specificity plot for ASL***

In terms of sensitivity of DSC [Figure 5], $I^2$ was noted to be high at 70%, indicating that more than a half of the variability between the studies was not due to random fluctuations. The between-study heterogeneity variance was estimated at $\tau^2$= 1.928. The pooled value of the sensitivity was 0.888 with a 95% CI = [0.638 - 0.973].

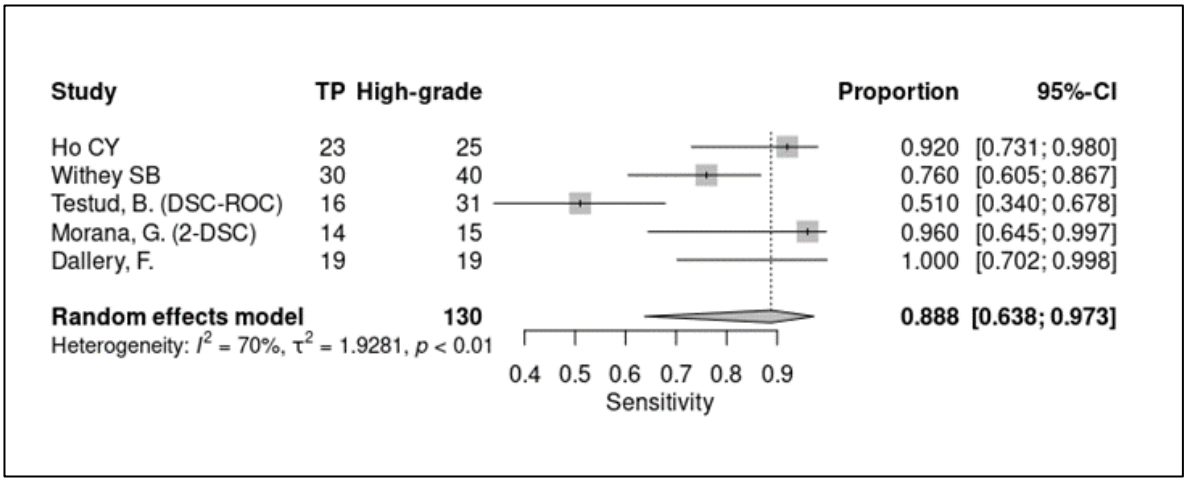


***Figure 5 - Sensitivity plot for DSC***

As noted with ASL, the heterogeneity among the DSC studies was greater for specificity than for sensitivity [Figure 6], at least as measured by $\tau^2$= 2.323. The $I^2$ value was practically the same at 69%, with this variance among the studies again noted to be significant ($p$ = 0.01). The pooled estimate of the specificity for these studies was 0.835 with a 95% CI = [0.512 - 0.960].

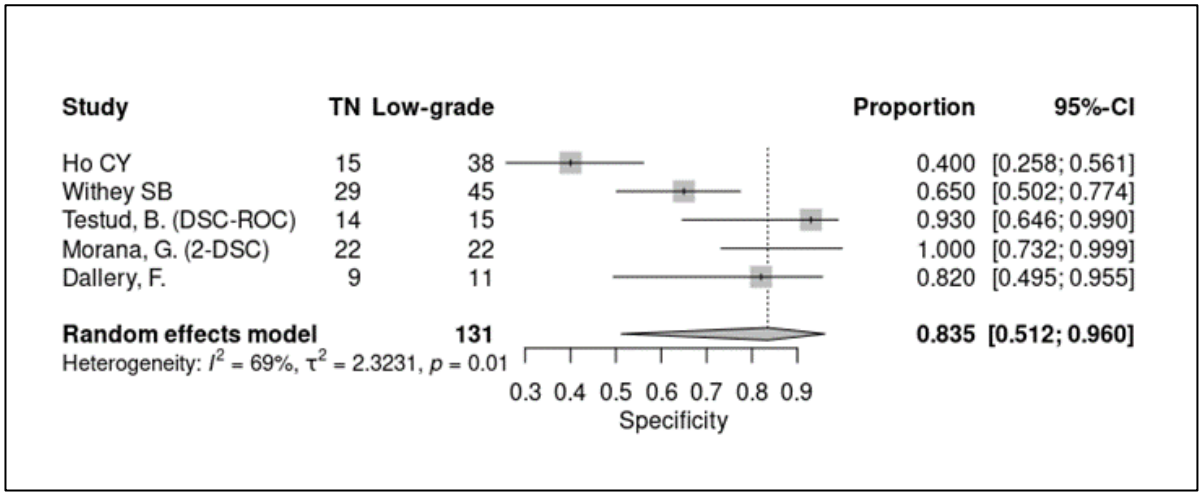


***Figure 6 - Specificity plot for DSC***

Moderator analyses could not be performed due to an insufficient number of studies. In view of the overall substantial heterogeneity, a random-effects model was used to merge statistics.

### 4.4.3 Crosshairs

The confidence intervals for all ASL and DSC datapoints in ROC space are presented in Figures 7 & 8 below. The heterogeneity in the DSC studies can once again be appreciated.

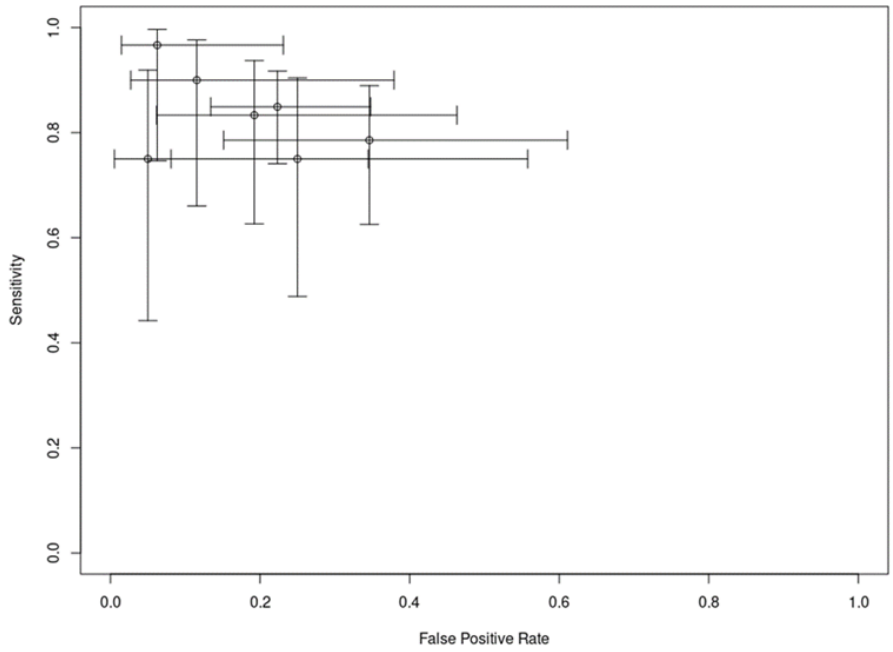


***Figure 7 - CI for all ASL data points in ROC space***

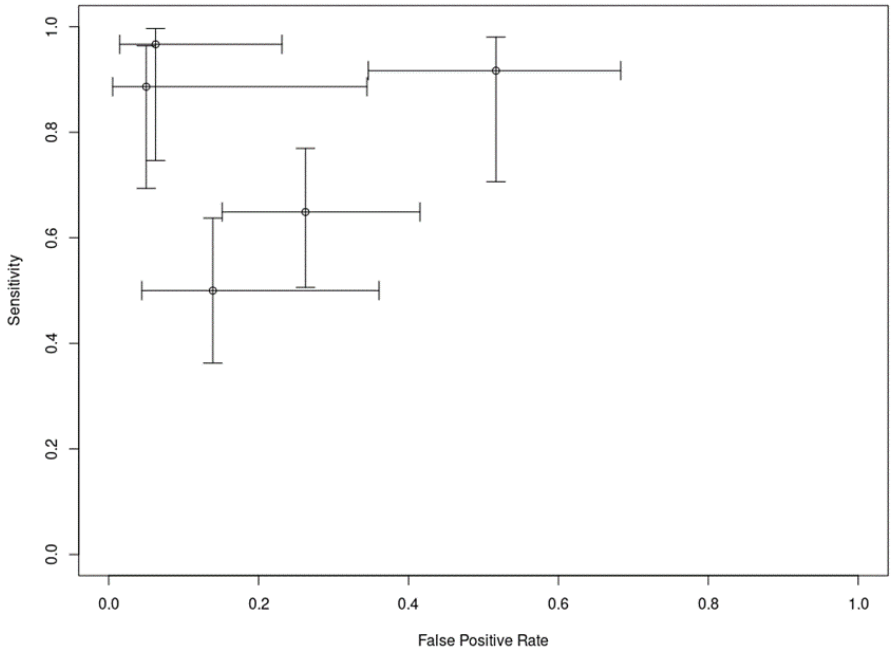


***Figure 8 - CI for all DSC data points in ROC space***

### 4.4.4 SROC curves

Meta-analysis of the ten studies using a bivariate model reitsma function was run with its default method of Restricted Maximum Likelihood (reml). The AUC for the summary ROC was estimated as 0.866. The point estimates for the pooled sensitivity and false positive rates were 0.798 and 0.201, respectively [Figure 9].

The Akaike information criterion (AIC) for the two summary plots were -22.487 for ASL and -4.416 for DSC. This indicates that the ASL plot is a better fit of the data, which is expected given that DSC data comprised a smaller number of studies, and also demonstrated greater heterogeneity [Figure 10].

ASL:

- Pooled AUC = 0.876
- Pooled Sensitivity = 0.824, 95% CI = [0.757 - 0.876]
- Pooled False positive rate = 0.204, 95% CI = [0.142 0.285]

DSC:

- Pooled AUC = 0.861
- Pooled Sensitivity = 0.789, 95% CI = [0.552 - 0.919]
- Pooled False positive rate = 0.203, 95% CI = [0.081 - 0.425]

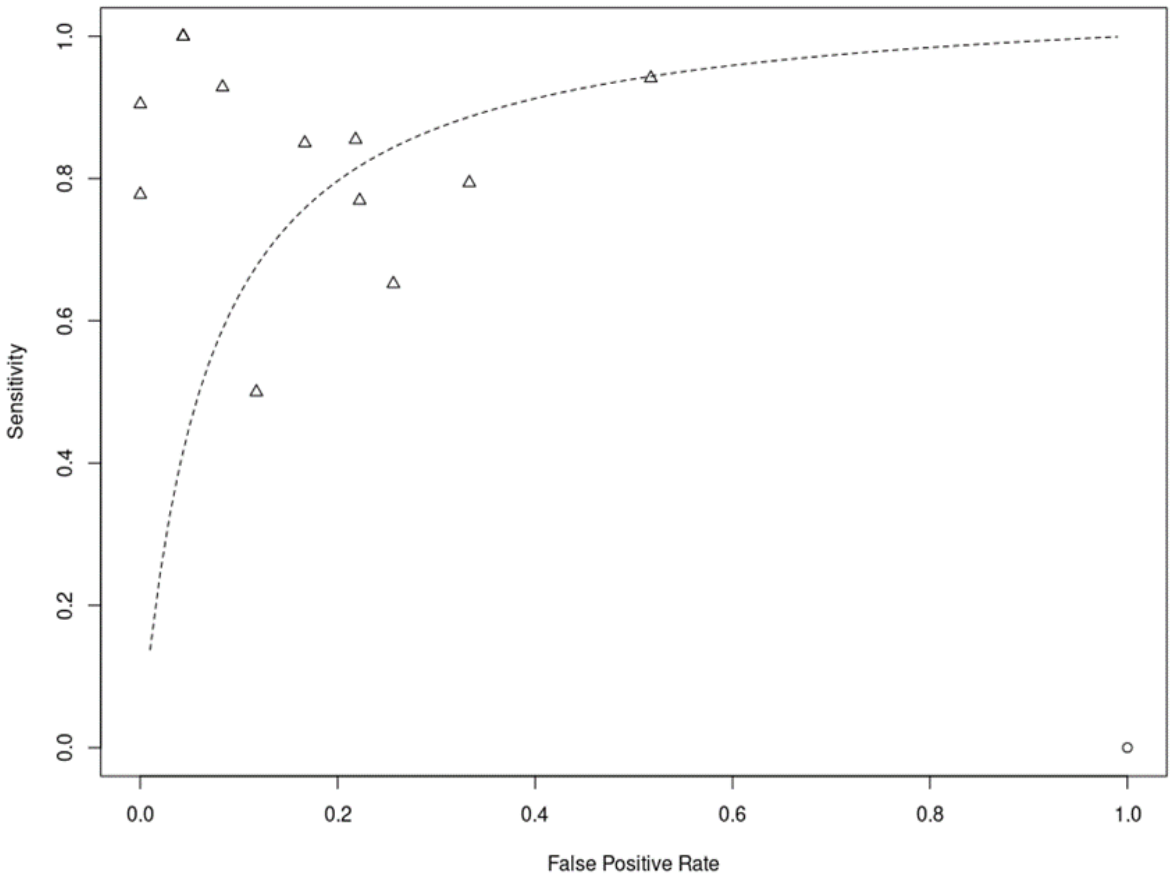


***Figure 9 - SROC curve (bivariate model) for all studies***

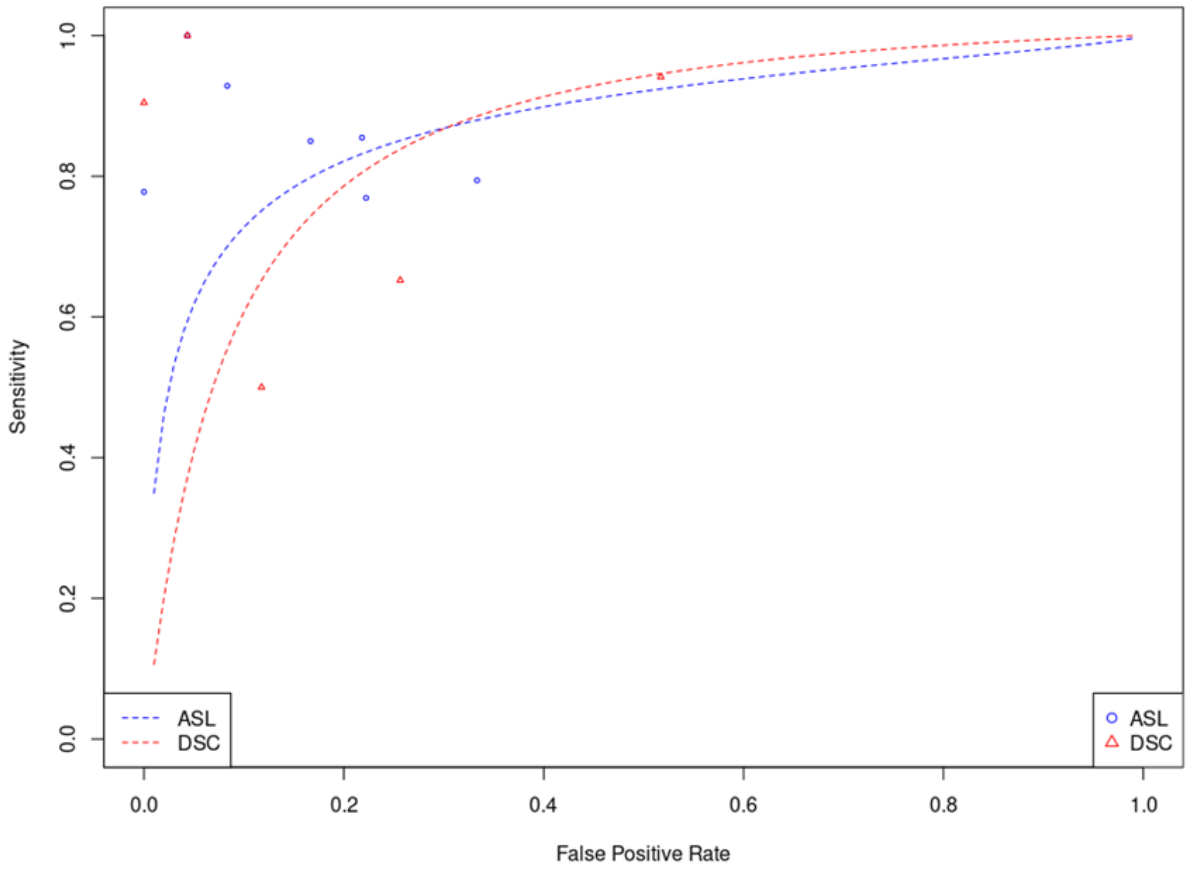


***Figure 10 - Comparison (bivariate) SROC of ASL and DSC***

# 5 Discussion

This metanalysis confirms that the application of ASL and DSC perfusion MRI confers a good diagnostic accuracy in distinguishing between low- and high-grade brain tumours in the paediatric population, with an AUC estimated at 0.866. This is clinically relevant given that a pre-operative indication of tumour grade is important to guide treatment decisions and strategies, as well as for prognostication.

DSC has been the traditionally used MR perfusion technique, being based on the quantification of susceptibility signal changes during the passage of exogenously administered contrast agent through the cerebral vasculature. Low-grade tumours are generally less vascularised than high-grade tumours, therefore the hemodynamic parameters measured by DSC, mainly CBV, would be expected to be significantly increased in the latter. This has in fact been shown in a number of studies as previously discussed. On analysis it was found that the pooled sensitivity and specificity of rCBV obtained by DSC to discriminate between low- and high-grade tumours was 78% and 80% respectively.

A limitation of this perfusion technique is the presence of leakage effects, the correction of which has led to a variety of approaches to obtain and process the obtained data. One such approach is the use of a contrast pre-load as has been discussed, however this is rarely done in children. The Boxerman consensus (Boxerman et al., 2006), advocates the application of leakage correction in the post-processing and provides guidance to that

effect. The approach to leakage correction was not well described in our studies and when it was, did vary somewhat across the studies that were included. Further standardisation needs to be implemented across different centres.

ASL is a non-invasive perfusion technique, based on using magnetically labelled arterial blood as an endogenous contrast tracer in order to measure blood flow. Unlike DSC, perfusion measurements in ASL are not tampered by blood-brain barrier permeability effects, giving a more accurate evaluation of tumour microcirculation and angiogenesis, and thus tumour grade. Furthermore, since shorter echo times are used, susceptibility effects leading to signal dropout and geometric distortions are less frequently encountered.

ASL does however suffer from low SNR and motion sensitivity. Additionally, measurement of absolute CBF is known to be unreliable due to variability in patient age, sex, haematocrit and cardiovascular status. However even when relative CBF is calculated, variation is still possible due to the difference in pulse sequences and post-processing algorithms which vary in between centres. Recently published consensus guidance regarding the most appropriate implementation for clinical applications and imaging parameters (Alsop et al., 2015) should standardise practice, however several of the included studies comprised cases that preceded these recommendations, also possibly accounting for a proportion of the heterogeneity that was noted. On analysis it was found that the pooled sensitivity and specificity of rCBF obtained by ASL to discriminate between low- and high-grade tumours was 82% and 80% respectively.

There have been a number of studies comparing the performance of ASL and DSC in brain tumour grading in adults (Ata et al., 2016; Cebeci et al., 2014; Hirai et al., 2011; Järnum et al., 2010; Luan et al., 2020; Rau et al., 2014; Warmuth et al., 2003; White et al., 2014), however given the different biology of paediatric brain tumours, extrapolation of adult study findings to this age group would be inappropriate.

The evidence on this topic in the paediatric population is unfortunately lacking. A recent study by Morana *et al.* noted this lacuna and demonstrated that ASL provides comparable results to DSC in paediatric astrocytic tumours, allowing distinction between low- and high-grade forms (Morana et al., 2018). A subsequent study noted moderate abilities of DSC and ASL to distinguish low- and high-grade paediatric brain tumours (Testud et al., 2021). There have not been any other such studies which directly compared ASL with DSC, however a number of studies have assessed each technique independently. Through a thorough systematic review, it was aimed to extract the diagnostic data from various studies and assess if there is a significant difference in the performance of these two techniques.

From our results it can be surmised that ASL seems to perform better, with a slightly higher pooled sensitivity than for DSC and with both giving the same pooled false positive rate. However, the difference between the two sensitivities was not statistically significant. The confidence interval of the estimate for ASL contains the point estimate for DSC, and vice-versa.

Substantial heterogeneity was noted in this study cohort. One reason for this could be the different tumour types and behaviours. In fact, the initial aim was to limit the analysis to

assessment of paediatric gliomas. However, during our search it was noted that a number of studies included other brain tumour types, albeit in much smaller numbers. Gliomas did however account for the majority of cases in our study population. Although the proportion of high versus low grade tumours was approximately equal in most studies, in one of the studies there were approximately double the number of high-grade tumours compared with low grade (Testud et al., 2021). Additionally, as previously alluded to, field strengths, parameter settings, post-processing methods and ROI measurement method varied across studies. These factors most likely contributed to the variations noted, however moderator analyses could not be performed due to an insufficient number of studies.

# 6 Conclusion and Recommendations

## 6.1 Strengths and Limitations

To our knowledge, this is the first systematic review with meta-analysis to collate and compare the available evidence regarding the diagnostic performance of both ASL and DSC in paediatric brain tumour grading.

A notable limitation of this review is the relatively small and heterogenous sample size. The small number of included studies is both a reflection of the limited research in this field, and also of the strict methodology standards which were adhered to in order to remain faithful to the review question. Incomplete inclusion of data in publications and lack of author response also contributed.

Nevertheless, neuro-oncological imaging is a continuously evolving field and further research in this regard needs to be undertaken, preferably using standardised scanning protocols to reduce heterogeneity. Harmonisation of imaging and interpretation techniques is key, leading to clearer comparison between studies with the potential downstream effect of generating a higher level of evidence.

Lastly, the majority of our studies defined the gold standard of tumour diagnostic assessment as histological/immunohistochemistry grading. However, as highlighted in the recent WHO classification update, the biological behaviour and prognosis of brain tumours is becoming increasingly defined through molecular profiling. This modification will need to be considered and evaluated in future studies.

## 6.2 Summary of Research

In this review, the accuracy of MR perfusion for differentiating primary untreated low-grade from high-grade brain tumours in paediatric patients was assessed.

Whilst DSC has been used more frequently than ASL in the evaluation of brain tumour grade in paediatric patients, the application of ASL is steadily increasing. ASL is a non-invasive technique and does not require the administration of gadolinium-based contrast agents.

As the diagnostic accuracy of ASL has been shown to be comparable and not inferior to DSC, its use in the diagnostic assessment of these patients should continue to be supported.

# References


Aboian, M. S., Solomon, D. A., Felton, E., Mabray, M. C., Villanueva-Meyer, J. E., Mueller, S., & Cha, S. (2017). Imaging Characteristics of Pediatric Diffuse Midline Gliomas with Histone H3 K27M Mutation. *American Journal of Neuroradiology*, *38*(4), 795–800. https://doi.org/10.3174/ajnr.A5076

Alsop, D. C., Detre, J. A., Golay, X., Günther, M., Hendrikse, J., Hernandez-Garcia, L., Lu, H., MacIntosh, B. J., Parkes, L. M., Smits, M., van Osch, M. J. P., Wang, D. J. J., Wong, E. C., & Zaharchuk, G. (2015). Recommended implementation of arterial spin-labeled perfusion MRI for clinical applications: A consensus of the ISMRM perfusion study group and the European consortium for ASL in dementia. *Magnetic Resonance in Medicine*, *73*(1), 102–116. https://doi.org/10.1002/mrm.25197

Ata, E. S., Turgut, M., Eraslan, C., & Dayanır, Y. Ö. (2016). Comparison between dynamic susceptibility contrast magnetic resonance imaging and arterial spin labeling techniques in distinguishing malignant from benign brain tumors. *European Journal of Radiology*, *85*(9), 1545–1553. https://doi.org/10.1016/j.ejrad.2016.05.015

Averill, L. W., & Kandula, V. V. R. (2017). Utility of Arterial Spin Labeling MRI in Pediatric Neuroimaging: A Pictorial Essay. *Current Radiology Reports*, *5*(8), 37. https://doi.org/10.1007/s40134-017-0232-x

Bandopadhayay, P., Bergthold, G., London, W. B., Goumnerova, L. C., Morales La Madrid, A., Marcus, K. J., Guo, D., Ullrich, N. J., Robison, N. J., Chi, S. N., Beroukhim, R., Kieran, M. W., & Manley, P. E. (2014). Long-term outcome of 4,040 children diagnosed with pediatric low-grade gliomas: An analysis of the Surveillance Epidemiology and End Results (SEER) database. *Pediatric Blood & Cancer*, *61*(7), 1173–1179. https://doi.org/10.1002/pbc.24958

Barkovich AJ. (2005). *Pediatric Neuroimaging* (4th ed.). Lippincott Williams & Wilkins.

Bender, K., Perez, E., Chirica, M., Onken, J., Kahn, J., Brenner, W., Ehret, F., Euskirchen, P., Koch, A., Capper, D., & Kaul, D. (2021). High-grade astrocytoma with piloid features (HGAP): the Charité experience with a new central nervous system tumor entity. *Journal of Neuro-Oncology*, *153*(1), 109–120. https://doi.org/10.1007/s11060-021-03749-z

Borja, M. J., Plaza, M. J., Altman, N., & Saigal, G. (2013). Conventional and Advanced MRI Features of Pediatric Intracranial Tumors: Supratentorial Tumors. *American Journal of Roentgenology*, *200*(5), W483–W503. https://doi.org/10.2214/AJR.12.9724

Boxerman, J. L., Schmainda, K. M., & Weisskoff, R. M. (2006). Relative cerebral blood volume maps corrected for contrast agent extravasation significantly correlate with glioma tumor grade, whereas uncorrected maps do not. *AJNR. American Journal of Neuroradiology*, *27*(4), 859–867.

Calamante, F. (2013). Arterial input function in perfusion MRI: A comprehensive review. *Progress in Nuclear Magnetic Resonance Spectroscopy*, *74*, 1–32. https://doi.org/10.1016/j.pnmrs.2013.04.002

Calamante, F., Mørup, M., & Hansen, L. K. (2004). Defining a local arterial input function for perfusion MRI using independent component analysis. *Magnetic Resonance in Medicine*, *52*(4), 789–797. https://doi.org/10.1002/mrm.20227

Cebeci, H., Aydin, O., Ozturk-Isik, E., Gumus, C., Inecikli, F., Bekar, A., Kocaeli, H., & Hakyemez, B. (2014). Assesment of perfusion in glial tumors with arterial spin labeling; comparison with dynamic susceptibility contrast method. *European Journal of Radiology*, *83*(10), 1914–1919. https://doi.org/10.1016/j.ejrad.2014.07.002

Cha, S. (2006). Dynamic Susceptibility-Weighted Contrast-Enhanced Perfusion MR Imaging in Pediatric Patients. *Neuroimaging Clinics of North America*, *16*(1), 137–147. https://doi.org/10.1016/j.nic.2005.11.006

Chen, W., Soon, Y. Y., Pratiseyo, P. D., Sutanto, R., Hendriansyah, L., Kuick, C. H., Chang, K. T. E., & Tan, C. L. (2020). Central nervous system neuroepithelial tumors with MN1-alteration: an individual patient data meta-analysis of 73 cases. *Brain Tumor Pathology*, *37*(4), 145–153. https://doi.org/10.1007/s10014-020-00372-0

Chen, Y., Tian, T., Guo, X., Zhang, F., Fan, M., Jin, H., & Liu, D. (2020). Polymorphous low-grade neuroepithelial tumor of the young: case report and review focus on the radiological features and genetic alterations. *BMC Neurology*, *20*(1), 123. https://doi.org/10.1186/s12883-020-01679-3

Clement, P., Petr, J., Dijsselhof, M. B. J., Padrela, B., Pasternak, M., Dolui, S., Jarutyte, L., Pinter, N., Hernandez-Garcia, L., Jahn, A., Kuijer, J. P. A., Barkhof, F., Mutsaerts, H. J. M. M., & Keil, V. C. (2022). A Beginner's Guide to Arterial Spin Labeling (ASL) Image Processing. *Frontiers in Radiology*, *2*. https://doi.org/10.3389/fradi.2022.929533

Dai, W., Garcia, D., de Bazelaire, C., & Alsop, D. C. (2008). Continuous flow-driven inversion for arterial spin labeling using pulsed radio frequency and gradient fields. *Magnetic Resonance in Medicine*, *60*(6), 1488–1497. https://doi.org/10.1002/mrm.21790

Dallery, F., Bouzerar, R., Michel, D., Attencourt, C., Promelle, V., Peltier, J., Constans, J. M., Balédent, O., & Gondry-Jouet, C. (2017). Perfusion magnetic resonance imaging in pediatric brain tumors. *Neuroradiology*, *59*(11), 1143–1153. https://doi.org/10.1007/s00234-017-1917-9

Dangouloff-Ros, V., Deroulers, C., Foissac, F., Badoual, M., Shotar, E., Grévent, D., Calmon, R., Pagès, M., Grill, J., Dufour, C., Blauwblomme, T., Puget, S., Zerah, M., Sainte-Rose, C., Brunelle, F., Varlet, P., & Boddaert, N. (2016). Arterial Spin Labeling to Predict Brain Tumor Grading in Children: Correlations between Histopathologic Vascular Density and Perfusion MR Imaging. *Radiology*, *281*(2), 553–566. https://doi.org/10.1148/radiol.2016152228

Delgado, A. F., De Luca, F., Hanagandi, P., van Westen, D., & Delgado, A. F. (2018). Arterial Spin-Labeling in Children with Brain Tumor: A Meta-Analysis. *American Journal of Neuroradiology*. https://doi.org/10.3174/ajnr.A5727

Doebler, P. S.-P. B. (2022). *mada: Meta-Analysis of Diagnostic Accuracy. https://CRAN.R-project.org/package=mada.*

Ellison, D. W., Aldape, K. D., Capper, D., Fouladi, M., Gilbert, M. R., Gilbertson, R. J., Hawkins, C., Merchant, T. E., Pajtler, K., Venneti, S., & Louis, D. N. (2020). cIMPACT-NOW update 7: advancing the molecular classification of ependymal tumors. *Brain Pathology*, bpa.12866. https://doi.org/10.1111/bpa.12866

Fangusaro, J. (2012). Pediatric High Grade Glioma: a Review and Update on Tumor Clinical Characteristics and Biology. *Frontiers in Oncology*, *2*. https://doi.org/10.3389/fonc.2012.00105

Farid, N., Almeida-Freitas, D. B., White, N. S., McDonald, C. R., Kuperman, J. M., Almutairi, A. A., Muller, K. A., VandenBerg, S. R., Kesari, S., & Dale, A. M. (2014). Combining diffusion and perfusion differentiates tumor from bevacizumab-related imaging abnormality (bria). *Journal of Neuro-Oncology*, *120*(3), 539–546. https://doi.org/10.1007/s11060-014-1583-2

Ferré, J.-C., Bannier, E., Raoult, H., Mineur, G., Carsin-Nicol, B., & Gauvrit, J.-Y. (2013). Arterial spin labeling (ASL) perfusion: Techniques and clinical use. *Diagnostic and Interventional Imaging*, *94*(12), 1211–1223. https://doi.org/10.1016/j.diii.2013.06.010

Fieselmann, A., Kowarschik, M., Ganguly, A., Hornegger, J., & Fahrig, R. (2011). Deconvolution-Based CT and MR Brain Perfusion Measurement: Theoretical Model Revisited and Practical Implementation Details. *International Journal of Biomedical Imaging*, *2011*, 1–20. https://doi.org/10.1155/2011/467563

Garcia, D. M., Duhamel, G., & Alsop, D. C. (2005). Efficiency of inversion pulses for background suppressed arterial spin labeling. *Magnetic Resonance in Medicine*, *54*(2), 366–372. https://doi.org/10.1002/mrm.20556

Golay, X., & Ho, M.-L. (2022). Multidelay ASL of the pediatric brain. *The British Journal of Radiology*, *95*(1134). https://doi.org/10.1259/bjr.20220034

Guerreiro Stucklin, A. S., Ryall, S., Fukuoka, K., Zapotocky, M., Lassaletta, A., Li, C., Bridge, T., Kim, B., Arnoldo, A., Kowalski, P. E., Zhong, Y., Johnson, M., Li, C., Ramani, A. K., Siddaway, R., Nobre, L. F., de Antonellis, P., Dunham, C., Cheng, S., … Hawkins, C. (2019). Alterations in ALK/ROS1/NTRK/MET drive a group of infantile hemispheric gliomas. *Nature Communications*, *10*(1), 4343. https://doi.org/10.1038/s41467-019-12187-5

Günther, M., Bock, M., & Schad, L. R. (2001). Arterial spin labeling in combination with a look-locker sampling strategy: Inflow turbo-sampling EPI-FAIR (ITS-FAIR). *Magnetic Resonance in Medicine*, *46*(5), 974–984. https://doi.org/10.1002/mrm.1284

Hales, P. W., d'Arco, F., Cooper, J., Pfeuffer, J., Hargrave, D., Mankad, K., & Clark, C. (2019). Arterial spin labelling and diffusion-weighted imaging in paediatric brain

tumours. *NeuroImage: Clinical*, *22*, 101696. https://doi.org/10.1016/j.nicl.2019.101696

Hales, P. W., Phipps, K. P., Kaur, R., & Clark, C. A. (2013). A Two-Stage Model for In Vivo Assessment of Brain Tumor Perfusion and Abnormal Vascular Structure Using Arterial Spin Labeling. *PLoS ONE*, *8*(10), e75717. https://doi.org/10.1371/journal.pone.0075717

Haller, S., Zaharchuk, G., Thomas, D. L., Lovblad, K.-O., Barkhof, F., & Golay, X. (2016). Arterial Spin Labeling Perfusion of the Brain: Emerging Clinical Applications. *Radiology*, *281*(2), 337–356. https://doi.org/10.1148/radiol.2016150789

Hipp, S. J., Steffen-Smith, E., Hammoud, D., Shih, J. H., Bent, R., & Warren, K. E. (2011). Predicting outcome of children with diffuse intrinsic pontine gliomas using multiparametric imaging. *Neuro-Oncology*, *13*(8), 904–909. https://doi.org/10.1093/neuonc/nor076

Hirai, T., Kitajima, M., Nakamura, H., Okuda, T., Sasao, A., Shigematsu, Y., Utsunomiya, D., Oda, S., Uetani, H., Morioka, M., & Yamashita, Y. (2011). Quantitative Blood Flow Measurements in Gliomas Using Arterial Spin-Labeling at 3T: Intermodality Agreement and Inter- and Intraobserver Reproducibility Study. *American Journal of Neuroradiology*, *32*(11), 2073–2079. https://doi.org/10.3174/ajnr.A2725

Ho, C. Y., Cardinal, J. S., Kamer, A. P., & Kralik, S. F. (2015). Relative cerebral blood volume from dynamic susceptibility contrast perfusion in the grading of pediatric primary brain tumors. *Neuroradiology*, *57*(3), 299–306. https://doi.org/10.1007/s00234-014-1478-0

Hu, L. S., Baxter, L. C., Pinnaduwage, D. S., Paine, T. L., Karis, J. P., Feuerstein, B. G., Schmainda, K. M., Dueck, A. C., Debbins, J., Smith, K. A., Nakaji, P., Eschbacher, J. M., Coons, S. W., & Heiserman, J. E. (2010). Optimized Preload Leakage-Correction Methods to Improve the Diagnostic Accuracy of Dynamic Susceptibility-Weighted Contrast-Enhanced Perfusion MR Imaging in Posttreatment Gliomas. *American Journal of Neuroradiology*, *31*(1), 40–48. https://doi.org/10.3174/ajnr.A1787

Jahng, G.-H., Li, K.-L., Ostergaard, L., & Calamante, F. (2014). Perfusion Magnetic Resonance Imaging: A Comprehensive Update on Principles and Techniques. *Korean Journal of Radiology*, *15*(5), 554. https://doi.org/10.3348/kjr.2014.15.5.554

Järnum, H., Steffensen, E. G., Knutsson, L., Fründ, E.-T., Simonsen, C. W., Lundbye-Christensen, S., Shankaranarayanan, A., Alsop, D. C., Jensen, F. T., & Larsson, E.-M. (2010). Perfusion MRI of brain tumours: a comparative study of pseudo-continuous arterial spin labelling and dynamic susceptibility contrast imaging. *Neuroradiology*, *52*(4), 307–317. https://doi.org/10.1007/s00234-009-0616-6

Jezzard, P., Chappell, M. A., & Okell, T. W. (2018). Arterial spin labeling for the measurement of cerebral perfusion and angiography. *Journal of Cerebral Blood Flow & Metabolism*, *38*(4), 603–626. https://doi.org/10.1177/0271678X17743240

Kanda, T., Fukusato, T., Matsuda, M., Toyoda, K., Oba, H., Kotoku, J., Haruyama, T., Kitajima, K., & Furui, S. (2015). Gadolinium-based Contrast Agent Accumulates in the Brain Even in Subjects without Severe Renal Dysfunction: Evaluation of Autopsy Brain Specimens with Inductively Coupled Plasma Mass Spectroscopy. *Radiology*, *276*(1), 228–232. https://doi.org/10.1148/radiol.2015142690

Kerner, D. M., Nikam, R., Kandula, V. V. R., & Averill, L. W. (2022). Pearls and Pitfalls in Arterial Spin Labeling Perfusion-Weighted Imaging in Clinical Pediatric Imaging. *Seminars in Ultrasound, CT and MRI*, *43*(1), 19–30. https://doi.org/10.1053/j.sult.2021.05.003

Kikuchi, K., Hiwatashi, A., Togao, O., Yamashita, K., Yoshimoto, K., Mizoguchi, M., Suzuki, S. O., Iwaki, T., Suzuki, Y., & Honda, H. (2017). Correlation between arterial spin-labeling perfusion and histopathological vascular density of pediatric intracranial tumors. *Journal of Neuro-Oncology*, *135*(3), 561–569. https://doi.org/10.1007/s11060-017-2604-8

Kitajima, M., & Uetani, H. (2023). Arterial Spin Labeling for Pediatric Central Nervous System Diseases: Techniques and Clinical Applications. *Magnetic Resonance in Medical Sciences*, *22*(1), rev.2021-0118. https://doi.org/10.2463/mrms.rev.2021-0118

Koob, M., Girard, N., Ghattas, B., Fellah, S., Confort-Gouny, S., Figarella-Branger, D., & Scavarda, D. (2016). The diagnostic accuracy of multiparametric MRI to determine pediatric brain tumor grades and types. *Journal of Neuro-Oncology*, *127*(2), 345–353. https://doi.org/10.1007/s11060-015-2042-4

Kurokawa, R., Baba, A., Emile, P., Kurokawa, M., Ota, Y., Kim, J., Capizzano, A., Srinivasan, A., & Moritani, T. (2022). Neuroimaging features of angiocentric glioma: A case series and systematic review. *Journal of Neuroimaging*, *32*(3), 389–399. https://doi.org/10.1111/jon.12983

Lacerda, S., & Law, M. (2009). Magnetic Resonance Perfusion and Permeability Imaging in Brain Tumors. *Neuroimaging Clinics of North America*, *19*(4), 527–557. https://doi.org/10.1016/j.nic.2009.08.007

Lannering, B., Sandström, P.-E., Holm, S., Lundgren, J., Pfeifer, S., Samuelsson, U., Strömberg, B., & Gustafsson, G. (2009). Classification, incidence and survival analyses of children with CNS tumours diagnosed in Sweden 1984-2005. *Acta Paediatrica*, *98*(10), 1620–1627. https://doi.org/10.1111/j.1651-2227.2009.01417.x

Law, M., Yang, S., Wang, H., Babb, J. S., Johnson, G., Cha, S., Knopp, E. A., & Zagzag, D. (2003). Glioma grading: sensitivity, specificity, and predictive values of perfusion MR imaging and proton MR spectroscopic imaging compared with conventional MR imaging. *AJNR. American Journal of Neuroradiology*, *24*(10), 1989–1998.

Law, M., Young, R., Babb, J., Pollack, E., & Johnson, G. (2007). Histogram analysis versus region of interest analysis of dynamic susceptibility contrast perfusion MR imaging data in the grading of cerebral gliomas. *AJNR. American Journal of Neuroradiology*, *28*(4), 761–766.

Leeflang, M. M., Deeks, J. J., Takwoingi, Y., & Macaskill, P. (2013). Cochrane diagnostic test accuracy reviews. *Systematic Reviews*, *2*(1), 82. https://doi.org/10.1186/2046-4053-2-82

Leu, K., Boxerman, J. L., & Ellingson, B. M. (2017). Effects of MRI Protocol Parameters, Preload Injection Dose, Fractionation Strategies, and Leakage Correction Algorithms on the Fidelity of Dynamic-Susceptibility Contrast MRI Estimates of Relative Cerebral Blood Volume in Gliomas. *American Journal of Neuroradiology*, *38*(3), 478–484. https://doi.org/10.3174/ajnr.A5027

Liu, H.-L., Chang, T.-T., Yan, F.-X., Li, C.-H., Lin, Y.-S., & Wong, A. M. (2015). Assessment of vessel permeability by combining dynamic contrast-enhanced and arterial spin labeling MRI. *NMR in Biomedicine*, *28*(6), 642–649. https://doi.org/10.1002/nbm.3297

Louis, D. N., Perry, A., Wesseling, P., Brat, D. J., Cree, I. A., Figarella-Branger, D., Hawkins, C., Ng, H. K., Pfister, S. M., Reifenberger, G., Soffietti, R., von Deimling, A., & Ellison, D. W. (2021). The 2021 WHO Classification of Tumors of the Central Nervous System: a summary. *Neuro-Oncology*, *23*(8), 1231–1251. https://doi.org/10.1093/neuonc/noab106

Luan, J., Wu, M., Wang, X., Qiao, L., Guo, G., & Zhang, C. (2020). The diagnostic value of quantitative analysis of ASL, DSC-MRI and DKI in the grading of cerebral gliomas: a meta-analysis. *Radiation Oncology*, *15*(1), 204. https://doi.org/10.1186/s13014-020-01643-y

Lucas, J. T., Knapp, B. J., Uh, J., Hua, C.-H., Merchant, T. E., Hwang, S. N., Patay, Z., & Broniscer, A. (2018). Posttreatment DSC-MRI is Predictive of Early Treatment Failure in Children with Supratentorial High-Grade Glioma Treated with Erlotinib. *Clinical Neuroradiology*, *28*(3), 393–400. https://doi.org/10.1007/s00062-017-0580-1

McDonald, R. J., McDonald, J. S., Kallmes, D. F., Jentoft, M. E., Murray, D. L., Thielen, K. R., Williamson, E. E., & Eckel, L. J. (2015). Intracranial Gadolinium Deposition after Contrast-enhanced MR Imaging. *Radiology*, *275*(3), 772–782. https://doi.org/10.1148/radiol.15150025

Moher, D., Liberati, A., Tetzlaff, J., & Altman, D. G. (2009). Preferred Reporting Items for Systematic Reviews and Meta-Analyses: The PRISMA Statement. *PLoS Medicine*, *6*(7), e1000097. https://doi.org/10.1371/journal.pmed.1000097

Morana, G., Piccardo, A., Tortora, D., Puntoni, M., Severino, M., Nozza, P., Ravegnani, M., Consales, A., Mascelli, S., Raso, A., Cabria, M., Verrico, A., Milanaccio, C., & Rossi, A. (2017). Grading and outcome prediction of pediatric diffuse astrocytic tumors with diffusion and arterial spin labeling perfusion MRI in comparison with 18F–DOPA PET. *European Journal of Nuclear Medicine and Molecular Imaging*, *44*(12), 2084–2093. https://doi.org/10.1007/s00259-017-3777-2

Morana, G., Tortora, D., Staglianò, S., Nozza, P., Mascelli, S., Severino, M., Piatelli, G., Consales, A., Lequin, M., Garrè, M. L., & Rossi, A. (2018). Pediatric astrocytic tumor grading: comparison between arterial spin labeling and dynamic susceptibility

contrast MRI perfusion. *Neuroradiology*, *60*(4), 437–446. https://doi.org/10.1007/s00234-018-1992-6

Morita, N., Wang, S., Chawla, S., Poptani, H., & Melhem, E. R. (2010). Dynamic susceptibility contrast perfusion weighted imaging in grading of nonenhancing astrocytomas. *Journal of Magnetic Resonance Imaging*, *32*(4), 803–808. https://doi.org/10.1002/jmri.22324

Osborn, A. G., Louis, D. N., Poussaint, T. Y., Linscott, L. L., & Salzman, K. L. (2022). The 2021 World Health Organization Classification of Tumors of the Central Nervous System: What Neuroradiologists Need to Know. *American Journal of Neuroradiology*, *43*(7), 928–937. https://doi.org/10.3174/ajnr.A7462

Østergaard, L., Weisskoff, R. M., Chesler, D. A., Gyldensted, C., & Rosen, B. R. (1996). High resolution measurement of cerebral blood flow using intravascular tracer bolus passages. Part I: Mathematical approach and statistical analysis. *Magnetic Resonance in Medicine*, *36*(5), 715–725. https://doi.org/10.1002/mrm.1910360510

Ostrom, Q. T., Patil, N., Cioffi, G., Waite, K., Kruchko, C., & Barnholtz-Sloan, J. S. (2020). CBTRUS Statistical Report: Primary Brain and Other Central Nervous System Tumors Diagnosed in the United States in 2013–2017. *Neuro-Oncology*, *22*(Supplement_1), iv1–iv96. https://doi.org/10.1093/neuonc/noaa200

Ouzzani, M., Hammady, H., Fedorowicz, Z., & Elmagarmid, A. (2016). Rayyan—a web and mobile app for systematic reviews. *Systematic Reviews*, *5*(1), 210. https://doi.org/10.1186/s13643-016-0384-4

Peet, A. C., Arvanitis, T. N., Leach, M. O., & Waldman, A. D. (2012). Functional imaging in adult and paediatric brain tumours. *Nature Reviews Clinical Oncology*, *9*(12), 700–711. https://doi.org/10.1038/nrclinonc.2012.187

Petrella, J. R., & Provenzale, J. M. (2000). MR Perfusion Imaging of the Brain. *American Journal of Roentgenology*, *175*(1), 207–219. https://doi.org/10.2214/ajr.175.1.1750207

Piccardo, A., Tortora, D., Mascelli, S., Severino, M., Piatelli, G., Consales, A., Pescetto, M., Biassoni, V., Schiavello, E., Massollo, M., Verrico, A., Milanaccio, C., Garrè, M. L., Rossi, A., & Morana, G. (2019). Advanced MR imaging and 18F-DOPA PET characteristics of H3K27M-mutant and wild-type pediatric diffuse midline gliomas. *European Journal of Nuclear Medicine and Molecular Imaging*, *46*(8), 1685–1694. https://doi.org/10.1007/s00259-019-04333-4

Pollack, I. F., & Jakacki, R. I. (2011). Childhood brain tumors: epidemiology, current management and future directions. *Nature Reviews Neurology*, *7*(9), 495–506. https://doi.org/10.1038/nrneurol.2011.110

Poretti, A., Meoded, A., & Huisman, T. A. G. M. (2012). Neuroimaging of pediatric posterior fossa tumors including review of the literature. *Journal of Magnetic Resonance Imaging*, *35*(1), 32–47. https://doi.org/10.1002/jmri.22722

Porto, L., Jurcoane, A., Schwabe, D., & Hattingen, E. (2014). Conventional magnetic resonance imaging in the differentiation between high and low-grade brain tumours

in paediatric patients. *European Journal of Paediatric Neurology*, *18*(1), 25–29. https://doi.org/10.1016/j.ejpn.2013.07.004

R Core Team. (2021). *R: A language and environment for statistical computing. R Foundation for Statistical Computing, Vienna, Austria. URL https://www.R-project.org/*.

Rau, M. K., Braun, C., Skardelly, M., Schittenhelm, J., Paulsen, F., Bender, B., Ernemann, U., & Bisdas, S. (2014). Prognostic value of blood flow estimated by arterial spin labeling and dynamic susceptibility contrast-enhanced MR imaging in high-grade gliomas. *Journal of Neuro-Oncology*, *120*(3), 557–566. https://doi.org/10.1007/s11060-014-1586-z

Reis, J., Stahl, R., Zimmermann, H., Ruf, V., Thon, N., Kunz, M., Liebig, T., & Forbrig, R. (2021). Advanced MRI Findings in Medulloblastomas: Relationship to Genetic Subtypes, Histopathology, and Immunohistochemistry. *Journal of Neuroimaging*, *31*(2), 306–316. https://doi.org/10.1111/jon.12831

Reitsma, J. B., Glas, A. S., Rutjes, A. W. S., Scholten, R. J. P. M., Bossuyt, P. M., & Zwinderman, A. H. (2005). Bivariate analysis of sensitivity and specificity produces informative summary measures in diagnostic reviews. *Journal of Clinical Epidemiology*, *58*(10), 982–990. https://doi.org/10.1016/j.jclinepi.2005.02.022

Richardson, W. S., Wilson, M. C., Nishikawa, J., & Hayward, R. S. (1995). The well-built clinical question: a key to evidence-based decisions. *ACP Journal Club*, *123*(3), A12-3.

Romano, A., Rossi Espagnet, M. C., Calabria, L. F., Coppola, V., Figà Talamanca, L., Cipriani, V., Minniti, G., Pierallini, A., Fantozzi, L. M., & Bozzao, A. (2012). Clinical applications of dynamic susceptibility contrast perfusion-weighted MR imaging in brain tumours. *La Radiologia Medica*, *117*(3), 445–460. https://doi.org/10.1007/s11547-011-0715-4

Rosen, B. R., Belliveau, J. W., & Chien, D. (1989). Perfusion imaging by nuclear magnetic resonance. *Magnetic Resonance Quarterly*, *5*(4), 263–281.

Ryall, S., Zapotocky, M., Fukuoka, K., Nobre, L., Guerreiro Stucklin, A., Bennett, J., Siddaway, R., Li, C., Pajovic, S., Arnoldo, A., Kowalski, P. E., Johnson, M., Sheth, J., Lassaletta, A., Tatevossian, R. G., Orisme, W., Qaddoumi, I., Surrey, L. F., Li, M. M., … Hawkins, C. (2020). Integrated Molecular and Clinical Analysis of 1,000 Pediatric Low-Grade Gliomas. *Cancer Cell*, *37*(4), 569-583.e5. https://doi.org/10.1016/j.ccell.2020.03.011

Schmainda, K. M., Rand, S. D., Joseph, A. M., Lund, R., Ward, B. D., Pathak, A. P., Ulmer, J. L., Badruddoja, M. A., & Krouwer, H. G. J. (2004). Characterization of a first-pass gradient-echo spin-echo method to predict brain tumor grade and angiogenesis. *AJNR. American Journal of Neuroradiology*, *25*(9), 1524–1532.

Shih, R. Y., & Koeller, K. K. (2018). Embryonal Tumors of the Central Nervous System: *From the Radiologic Pathology Archives*. *RadioGraphics*, *38*(2), 525–541. https://doi.org/10.1148/rg.2018170182

Shin, J. H., Lee, H. K., Kwun, B. D., Kim, J.-S., Kang, W., Choi, C. G., & Suh, D. C. (2002). Using Relative Cerebral Blood Flow and Volume to Evaluate the Histopathologic Grade of Cerebral Gliomas: Preliminary Results. *American Journal of Roentgenology*, *179*(3), 783–789. https://doi.org/10.2214/ajr.179.3.1790783

Simonsen, C. Z., Ostergaard, L., Smith, D. F., Vestergaard-Poulsen, P., & Gyldensted, C. (2000). Comparison of gradient- and spin-echo imaging: CBF, CBV, and MTT measurements by bolus tracking. *Journal of Magnetic Resonance Imaging*, *12*(3), 411–416. https://doi.org/10.1002/1522-2586(200009)12:3<411::AID-JMRI6>3.0.CO;2-5

Surveillance Epidemiology and End Results (SEER) Program. (2019). *SEER*Stat Database: Mortality - All COD, Aggregated With State, Total U.S. (1969-2017) <Katrina/Rita Population Adjustment>, National Cancer Institute, DCCPS, Surveillance Research Program. Underlying mortality data provided by NCHS; (www.cdc.gov/nchs).*

Testud, B., Brun, G., Varoquaux, A., Hak, J. F., Appay, R., Le Troter, A., Girard, N., & Stellmann, J. P. (2021). Perfusion-weighted techniques in MRI grading of pediatric cerebral tumors: efficiency of dynamic susceptibility contrast and arterial spin labeling. *Neuroradiology*, *63*(8), 1353–1366. https://doi.org/10.1007/s00234-021-02640-y

Udaka, Y. T., & Packer, R. J. (2018). Pediatric Brain Tumors. *Neurologic Clinics*, *36*(3), 533–556. https://doi.org/10.1016/j.ncl.2018.04.009

Vidyasagar, R., Abernethy, L., Pizer, B., Avula, S., & Parkes, L. M. (2016). Quantitative measurement of blood flow in paediatric brain tumours—a comparative study of dynamic susceptibility contrast and multi time-point arterial spin labelled MRI. *The British Journal of Radiology*, *89*(1062), 20150624. https://doi.org/10.1259/bjr.20150624

Viechtbauer, W. (2010). Conducting Meta-Analyses in R with the metafor Package. *Journal of Statistical Software*, *36*(3). https://doi.org/10.18637/jss.v036.i03

Wang, D. J. J., Alger, J. R., Qiao, J. X., Gunther, M., Pope, W. B., Saver, J. L., Salamon, N., & Liebeskind, D. S. (2013). Multi-delay multi-parametric arterial spin-labeled perfusion MRI in acute ischemic stroke — Comparison with dynamic susceptibility contrast enhanced perfusion imaging. *NeuroImage: Clinical*, *3*, 1–7. https://doi.org/10.1016/j.nicl.2013.06.017

Warmuth, C., Günther, M., & Zimmer, C. (2003). Quantification of Blood Flow in Brain Tumors: Comparison of Arterial Spin Labeling and Dynamic Susceptibility-weighted Contrast-enhanced MR Imaging. *Radiology*, *228*(2), 523–532. https://doi.org/10.1148/radiol.2282020409

Wen, P. Y., Stein, A., van den Bent, M., De Greve, J., Wick, A., de Vos, F. Y. F. L., von Bubnoff, N., van Linde, M. E., Lai, A., Prager, G. W., Campone, M., Fasolo, A., Lopez-Martin, J. A., Kim, T. M., Mason, W. P., Hofheinz, R.-D., Blay, J.-Y., Cho, D. C., Gazzah, A., … Subbiah, V. (2022). Dabrafenib plus trametinib in patients with BRAFV600E-mutant low-grade and high-grade glioma (ROAR): a multicentre,

open-label, single-arm, phase 2, basket trial. *The Lancet Oncology*, *23*(1), 53–64. https://doi.org/10.1016/S1470-2045(21)00578-7

White, C. M., Pope, W. B., Zaw, T., Qiao, J., Naeini, K. M., Lai, A., Nghiemphu, P. L., Wang, J. J., Cloughesy, T. F., & Ellingson, B. M. (2014). Regional and voxel-wise comparisons of blood flow measurements between dynamic susceptibility contrast magnetic resonance imaging (DSC-MRI) and arterial spin labeling (ASL) in brain tumors. *Journal of Neuroimaging : Official Journal of the American Society of Neuroimaging*, *24*(1), 23–30. https://doi.org/10.1111/j.1552-6569.2012.00703.x

Whiting, P. F. (2011). QUADAS-2: A Revised Tool for the Quality Assessment of Diagnostic Accuracy Studies. *Annals of Internal Medicine*, *155*(8), 529. https://doi.org/10.7326/0003-4819-155-8-201110180-00009

WHO Classification of Tumours Editorial Board. (2021). *World Health Organization Classification of Tumours of the Central Nervous System.: Vol. Volume 6* (5th edition).

Williams, D. S., Detre, J. A., Leigh, J. S., & Koretsky, A. P. (1992). Magnetic resonance imaging of perfusion using spin inversion of arterial water. *Proceedings of the National Academy of Sciences*, *89*(1), 212–216. https://doi.org/10.1073/pnas.89.1.212

Withey, S. B., MacPherson, L., Oates, A., Powell, S., Novak, J., Abernethy, L., Pizer, B., Grundy, R., Morgan, P. S., Bailey, S., Mitra, D., Arvanitis, T. N., Auer, D. P., Avula, S., & Peet, A. C. (2022). Dynamic susceptibility-contrast magnetic resonance imaging with contrast agent leakage correction aids in predicting grade in pediatric brain tumours: a multicenter study. *Pediatric Radiology*, *52*(6), 1134–1149. https://doi.org/10.1007/s00247-021-05266-7

Wolf, R. L., Wang, J., Wang, S., Melhem, E. R., O'Rourke, D. M., Judy, K. D., & Detre, J. A. (2005). Grading of CNS neoplasms using continuous arterial spin labeled perfusion MR imaging at 3 Tesla. *Journal of Magnetic Resonance Imaging*, *22*(4), 475–482. https://doi.org/10.1002/jmri.20415

Ye, F. Q., Mattay, V. S., Jezzard, P., Frank, J. A., Weinberger, D. R., & McLaughlin, A. C. (1997). Correction for vascular artifacts in cerebral blood flow values measured by using arterial spin tagging techniques. *Magnetic Resonance in Medicine*, *37*(2), 226–235. https://doi.org/10.1002/mrm.1910370215

Yeom, K. W., Mitchell, L. A., Lober, R. M., Barnes, P. D., Vogel, H., Fisher, P. G., & Edwards, M. S. (2014). Arterial Spin-Labeled Perfusion of Pediatric Brain Tumors. *American Journal of Neuroradiology*, *35*(2), 395–401. https://doi.org/10.3174/ajnr.A3670

# Appendices

## Appendix 1

### Pubmed Search Strategy

| Search number | Query | Sort By | Filters | Search Details | Results | Time |
|---|---|---|---|---|---|---|
| 5 | #1 AND #2 AND #3 | | in the last 10 years | ((((("Glioma"[All Fields] OR "neoplasm"[All Fields] OR "neoplasia"[All Fields] OR "tumor"[All Fields] OR "tumour"[All Fields] OR "cancer"[All Fields] OR "malignancy"[All Fields]) AND "Brain"[All Fields]) OR "Central Nervous System"[All Fields] OR "Cerebral"[All Fields] OR "intracranial"[All Fields] OR "Glial"[All Fields]) AND ("paediatric"[All Fields] OR "pediatric"[All Fields] OR "young adult"[All Fields] OR "infant"[All Fields] OR "child"[All Fields] OR "children"[All Fields] OR "adolescent"[All Fields]) AND ("perfusion"[All Fields] OR "ASL"[All Fields] OR "arterial spin labelling"[All Fields] OR "arterial spin labeling"[All Fields] OR "arterial spin labeled"[All Fields] OR "dynamic susceptibility contrast"[All Fields] OR "DSC"[All Fields] OR "Perfusion Weighted MRI"[All Fields] OR "MR Perfusion"[All Fields] OR "MRI Perfusion"[All Fields] OR "Spin Labels"[All Fields])) AND (y_10[Filter]) | 2,826 | 12:58:29 |
| 4 | #1 AND #2 AND #3 | | | (((("Glioma"[All Fields] OR "neoplasm"[All Fields] OR "neoplasia"[All Fields] OR "tumor"[All Fields] OR "tumour"[All Fields] OR "cancer"[All Fields] OR "malignancy"[All Fields]) AND "Brain"[All Fields]) OR "Central Nervous System"[All Fields] OR "Cerebral"[All Fields] OR "intracranial"[All Fields] OR "Glial"[All Fields]) AND ("paediatric"[All Fields] OR "pediatric"[All Fields] OR "young adult"[All Fields] OR "infant"[All Fields] OR "child"[All Fields] OR "children"[All Fields] OR "adolescent"[All Fields]) AND ("perfusion"[All Fields] OR "ASL"[All Fields] OR | 5,742 | 12:58:18 |

| | | | | | |
|---|---|---|---|---|---|
| | | | **"arterial spin labelling"[All Fields] OR "arterial spin labeling"[All Fields] OR "arterial spin labeled"[All Fields] OR "dynamic susceptibility contrast"[All Fields] OR "DSC"[All Fields] OR "Perfusion Weighted MRI"[All Fields] OR "MR Perfusion"[All Fields] OR "MRI Perfusion"[All Fields] OR "Spin Labels"[All Fields])** | | |
| **3** | **("perfusion" OR "ASL" OR "arterial spin labelling" OR "arterial spin labeling" OR "arterial spin labeled" OR "dynamic susceptibility contrast" OR "DSC" OR "Perfusion Weighted MRI" OR "MR Perfusion" OR "MRI Perfusion" OR "Spin Labels")** | | **"perfusion"[All Fields] OR "ASL"[All Fields] OR "arterial spin labelling"[All Fields] OR "arterial spin labeling"[All Fields] OR "arterial spin labeled"[All Fields] OR "dynamic susceptibility contrast"[All Fields] OR "DSC"[All Fields] OR "Perfusion Weighted MRI"[All Fields] OR "MR Perfusion"[All Fields] OR "MRI Perfusion"[All Fields] OR "Spin Labels"[All Fields]** | **252,240** | **12:57:39** |
| **2** | **("paediatric" OR "pediatric" OR "young adult" OR "infant" OR "child" OR "children" OR "adolescent")** | | **"paediatric"[All Fields] OR "pediatric"[All Fields] OR "young adult"[All Fields] OR "infant"[All Fields] OR "child"[All Fields] OR "children"[All Fields] OR "adolescent"[All Fields]** | **5,112,674** | **12:55:43** |
| **1** | **"Glioma" OR "neoplasm" OR "neoplasia" OR "tumor" OR "tumour" OR "cancer" OR "malignancy" AND "Brain" OR "Central Nervous System" OR "Cerebral" OR "intracranial" OR "Glial"** | | **(("Glioma"[All Fields] OR "neoplasm"[All Fields] OR "neoplasia"[All Fields] OR "tumor"[All Fields] OR "tumour"[All Fields] OR "cancer"[All Fields] OR "malignancy"[All Fields]) AND "Brain"[All Fields]) OR "Central Nervous System"[All Fields] OR "Cerebral"[All Fields] OR "intracranial"[All Fields] OR "Glial"[All Fields]** | **1,141,019** | **12:55:19** |

| Search number | Query | Sort By | Filters | Search Details | Results | Time |
|---|---|---|---|---|---|---|
| 5 | #1 AND #2 AND #3 | in the last 10 years | | ((((("Glioma"[All Fields] OR "neoplasm"[All Fields] OR "neoplasia"[All Fields] OR "tumor"[All Fields] OR "tumour"[All Fields] OR "cancer"[All Fields] OR "malignancy"[All Fields]) AND "Brain"[All Fields]) OR "Central Nervous System"[All Fields] OR "Cerebral"[All Fields] OR "intracranial"[All Fields] OR "Glial"[All Fields]) AND ("paediatric"[All Fields] OR "pediatric"[All Fields] OR "young adult"[All Fields] OR "infant"[All Fields] OR "child"[All Fields] OR "children"[All Fields] OR "adolescent"[All Fields]) AND ("perfusion"[All Fields] OR "ASL"[All Fields] OR "arterial spin labelling"[All Fields] OR "arterial spin labeling"[All Fields] OR "arterial spin labeled"[All Fields] OR "dynamic susceptibility contrast"[All Fields] OR "DSC"[All Fields] OR "Perfusion Weighted MRI"[All Fields] OR "MR Perfusion"[All Fields] OR "MRI Perfusion"[All Fields] OR "Spin Labels"[All Fields])) AND (y_10[Filter]) | 2,826 | 12:58:29 |
| 4 | #1 AND #2 AND #3 | | | ((("Glioma"[All Fields] OR "neoplasm"[All Fields] OR "neoplasia"[All Fields] OR "tumor"[All Fields] OR "tumour"[All Fields] OR "cancer"[All Fields] OR "malignancy"[All Fields]) AND "Brain"[All Fields]) OR "Central Nervous System"[All Fields] OR "Cerebral"[All Fields] OR "intracranial"[All Fields] OR "Glial"[All Fields]) AND ("paediatric"[All Fields] OR "pediatric"[All Fields] OR "young adult"[All Fields] OR "infant"[All Fields] OR "child"[All Fields] OR "children"[All Fields] OR "adolescent"[All Fields]) AND ("perfusion"[All Fields] OR "ASL"[All Fields] OR "arterial spin labelling"[All Fields] OR "arterial spin labeling"[All Fields] OR "arterial spin labeled"[All Fields] OR "dynamic susceptibility contrast"[All Fields] OR "DSC"[All Fields] OR "Perfusion Weighted MRI"[All Fields] OR "MR Perfusion"[All Fields] OR | 5,742 | 12:58:18 |

| | | | | | |
|---|---|---|---|---|---|
| | | | "MRI Perfusion"[All Fields] OR "Spin Labels"[All Fields]) | | |
| 3 | ("perfusion" OR "ASL" OR "arterial spin labelling" OR "arterial spin labeling" OR "arterial spin labeled" OR "dynamic susceptibility contrast" OR "DSC" OR "Perfusion Weighted MRI" OR "MR Perfusion" OR "MRI Perfusion" OR "Spin Labels") | | "perfusion"[All Fields] OR "ASL"[All Fields] OR "arterial spin labelling"[All Fields] OR "arterial spin labeling"[All Fields] OR "arterial spin labeled"[All Fields] OR "dynamic susceptibility contrast"[All Fields] OR "DSC"[All Fields] OR "Perfusion Weighted MRI"[All Fields] OR "MR Perfusion"[All Fields] OR "MRI Perfusion"[All Fields] OR "Spin Labels"[All Fields] | 252,240 | 12:57:39 |
| 2 | ("paediatric" OR "pediatric" OR "young adult" OR "infant" OR "child" OR "children" OR "adolescent") | | "paediatric"[All Fields] OR "pediatric"[All Fields] OR "young adult"[All Fields] OR "infant"[All Fields] OR "child"[All Fields] OR "children"[All Fields] OR "adolescent"[All Fields] | 5,112,674 | 12:55:43 |
| 1 | "Glioma" OR "neoplasm" OR "neoplasia" OR "tumor" OR "tumour" OR "cancer" OR "malignancy" AND "Brain" OR "Central Nervous System" OR "Cerebral" OR "intracranial" OR "Glial" | | (("Glioma"[All Fields] OR "neoplasm"[All Fields] OR "neoplasia"[All Fields] OR "tumor"[All Fields] OR "tumour"[All Fields] OR "cancer"[All Fields] OR "malignancy"[All Fields]) AND "Brain"[All Fields]) OR "Central Nervous System"[All Fields] OR "Cerebral"[All Fields] OR "intracranial"[All Fields] OR "Glial"[All Fields] | 1,141,019 | 12:55:19 |

## Appendix 2

### Web of Science Search Strategy

# Database: Web of Science Core Collection

# Entitlements:

- WOS.SSCI: 1994 to 2022

- WOS.AHCI: 1994 to 2022

- WOS.ISTP: 1997 to 2022

- WOS.ESCI: 2017 to 2022

- WOS.SCI: 1994 to 2022

- WOS.ISSHP: 1997 to 2022

# Searches:

1: ((ALL=((“Glioma” OR “neoplasm” OR “neoplasia” OR “tumor” OR “tumour” OR “cancer” OR “malignancy” AND “Brain” OR “Central Nervous System” OR “Cerebral” OR “intracranial” OR “Glial”))) AND ALL=((“paediatric” OR “pediatric” OR “young adult” OR “infant” OR “child” OR “children” OR “adolescent”))) AND ALL=((“perfusion” OR “ASL” OR “arterial spin labelling” OR “arterial spin labeling” OR “arterial spin labeled” OR “dynamic susceptibility contrast” OR “DSC” OR “Perfusion Weighted MRI” OR “MR Perfusion” OR “MRI Perfusion” OR “Spin Labels”)) Timespan: 2012-01-01 to 2022-08-01 Date run: Fri Aug 05 2022 19:28:03 GMT+0200 (Central European Summer Time)

Results: 2266

## Appendix 3

### SCOPUS Search Strategy

( ALL ( ( "Glioma" OR "neoplasm" OR "neoplasia" OR "tumor" OR "tumour" OR "cancer" OR "malignancy" AND "Brain" OR "Central Nervous System" OR "Cerebral" OR "intracranial" OR "Glial" ) ) AND ALL ( ( "paediatric" OR "pediatric" OR "young adult" OR "infant" OR "child" OR "children" OR "adolescent" ) ) AND ALL ( ( "perfusion" OR "ASL" OR "arterial spin labelling" OR "arterial spin labeling" OR "arterial spin labeled" OR "dynamic susceptibility contrast" OR "DSC" OR "Perfusion Weighted MRI" OR "MR Perfusion" OR "MRI Perfusion" OR "Spin Labels" ) ) ) AND PUBYEAR > 2011 AND ( LIMIT-TO ( PUBYEAR , 2023 ) OR LIMIT-TO ( PUBYEAR , 2022 ) ) AND ( LIMIT-TO ( SUBJAREA , "MEDI" ) OR LIMIT-TO ( SUBJAREA , "BIOC" ) OR LIMIT-TO ( SUBJAREA , "NEUR" ) )

Results: 1822